Correlations Describing Laminar Hydrodynamic Development in a Circular Pipe

KENAN KAYA[1*] and OKTAY ÖZCAN[2]

[1]*Department of Mechanical Engineering, Faculty of Engineering, Istanbul Aydin University, Kucukcekmece, 34295 Istanbul, Turkey*

[2]*Department of Aeronautical Engineering, Faculty of Engineering and Architecture, Istanbul Gelisim University, Avcilar, 34310 Istanbul, Turkey*

**Corresponding author. Tel: +905362263279*
E-mail address: kenankaya@aydin.edu.tr

ABSTRACT

Computational Fluid Dynamics (CFD) is employed to study incompressible and steady laminar flow in the hydrodynamic entrance region of circular pipes for a wide range of Reynolds numbers. Dimensionless analytic expressions for streamwise variations of the centerline velocity, skin friction coefficient and pressure drop are derived by applying a two-stage nonlinear regression analysis to computational solutions of the Navier-Stokes equations for various Reynolds numbers between 1 and 2000. Similar expressions are also presented for the correction factors for the momentum and kinetic energy fluxes. Firstly, the correlation parameters for a flow variable are obtained for each Reynolds number considered. Subsequently, a second nonlinear regression analysis is conducted to obtain another set of equations for the variation of fitting parameters with the Reynolds number. Constant parameter correlations are also given for the Reynolds number range between 200 and 2000, which are less accurate than the expressions containing Reynolds number dependent terms. The correlations presented here are also valid for flows with heat transfer, under the assumptions of constant property and zero buoyancy.

1. INTRODUCTION

The hydrodynamic development of incompressible laminar flow in a circular pipe has been the subject of many studies historically. The characteristics of flow development are of interest not only for scientific but also for practical applications, such as the design of

compact heat exchangers **[1, 2]**, and microfluidic devices **[3–6]**. Hydrodynamically fully developed flow, which is characterized by the streamwise (axial, longitudinal) invariance of the velocity profiles and skin-friction, has a well-known parabolic velocity solution **[7–9]**. The streamwise development of the velocity has been studied by i) momentum integral methods **[10–13]**; ii) analytical solutions of the linearized momentum equation **[14],** iii) numerical solutions of the ‘‘boundary-layer approximation’’ equations, which neglect axial diffusion and radial pressure variation **[15]**; and iv) solving the Navier-Stokes equations **[16–20]**. An extensive survey of the previous work on thermal and hydrodynamic flow developments in a circular pipe is presented in **[1]**. **Reci et al**. **[21]** present the results of a recent experimental study on hydrodynamic development. Based on a scaling analysis, **Muzychka and Yovanovich [22]** propose the square root of cross-sectional area as a new length scale for flow development in ducts and present a correlation for the friction coefficient. Experimental results obtained by **Sharp and Adrian [6]** in microtubes confirm the validity of Poiseuille flow pressure drop relations in a fully developed microscale flow. **Gad-el-Hak [23]** discusses the compressibility effects, boundary conditions and the validity limits of the continuum approximation in microscale flows. **Duan and Muzychka [24]** present an analytical solution of the ‘‘boundary-layer approximation’’ equations for the developing pipe flow in both the continuum and slip-flow regimes.

Velocity profiles in the flow development region are presented by **Hornbeck [15], Durst et al. [20]** and **Shah and Bhatti [25].** These profiles are solutions of the boundary-layer approximation equations which are non-dimensionalized in terms of $x^+=x/(\mathrm{Re})D$ (x is the axial distance measured from pipe inlet and Re is the Reynolds number based on the pipe diameter, D) and independent of the Reynolds number. **Shimomukai and Kanda [16]** present velocity profiles obtained by solutions of the Navier-Stokes equations whose dimensionless form contains the Reynolds number. The Navier-Stokes solution of **Shimomukai and Kanda**

[16] at Re=2000 is in reasonably good agreement with the ‘‘boundary-layer approximation’’ solution of **Hornbeck [15].** **Shah and Bhatti [25]** note that the effects of the axial momentum diffusion and radial pressure variation, which are neglected in the ‘‘boundary-layer approximation’’ are important very near the duct inlet ($x^+ < 0.005$) for Re < 400. **Durst et al. [20]** provide analytic expressions for the development length into the fully developed state.

The effect of inlet conditions on the transitional flow development in circular pipes and rectangular channels has been reported by **Haustein and Kashi [11]**, **Tam and Ghajar [26]** and **Rehman et al. [5]**, respectively. **Haustein and Kashi [11]** report that the sharp corner inlet solution reveals the well-known vena contracta phenomenon for Re > 320, and the solution relaxes back to the ideal inlet solution for $x^+ > 0.01$ at Re = 2000. Microchannel studies by **Tam and Ghajar [26]** and **Rehman et al. [5]** find that the bell-mouth entry increases the value of the critical Reynolds number.

Correlations for axial variation of the Nusselt number along a pipe are available in the literature **[1, 25].** Correlations for streamwise variation of pressure drop are given by **Shah and London [1]**, and **Shah [2]**. However, there is a lack of published studies offering expressions for streamwise variations of skin-friction, centerline velocity, and pressure drop. Integral flow parameters such as momentum and kinetic energy correction factors (β and α) provide information on the development stage of the velocity field. Streamwise variation of such integral parameters in laminar axisymmetric pipe flow has also not been reported in the literature.

This study discusses momentum transfer in the developing flow region of a smooth circular pipe (with a uniform velocity inlet) using numerical solutions of the laminar incompressible steady Navier-Stokes equations; and provides analytic expressions that describe the streamwise development of the hydrodynamic variables such as skin-friction, centerline

velocity, and pressure gradient (all in dimensionless form) for a wide range of Reynolds numbers (from 1 to 2000). In Section 2, the Navier-Stokes equations are presented, and the nonlinear regression procedure for obtaining the correlations is described. Verification and validation of the numerical procedure are discussed in Sec. 3. Results for the developing velocity field, as well as the streamwise development of all flow parameters toward the fully developed values are presented and discussed in Sec. 4. A summary of the results and conclusions is presented in Sec. 5.

The primary novelty of this study is that it addresses a knowledge gap for the relatively lower Reynolds numbers considered here; as the Reynolds numbers of Re = 1, 2, 3, 4, 6, 8, 10, 16, 20, 25, 30, 36, 40, 50, 70, 100, 140, 200, 250, 300, 500, 700, 1000, 1500 and 2000 are studied. The complete Navier-Stokes equations without any simplifications or assumptions (i. e., without neglecting the axial diffusion, radial component of velocity, and radial variation in pressure) are solved numerically, and highly accurate analytical expressions for the streamwise variation of some selected flow variables are provided. The results of the numerical calculations are verified by comparison with theoretical data and those reported in some previous studies.

2. PIPE FLOW EQUATIONS, INTEGRAL PARAMETERS AND NONLINEAR REGRESSION

Flow in a circular duct is axisymmetric if the boundary conditions and momentum or heat sources are symmetrical with respect to the axis of rotation. The Navier-Stokes equations in the cylindrical coordinates, arranged for incompressible and steady laminar axisymmetric flow, govern the type of problems considered in this study; and can be found in many textbooks **[7–9]**. The dimensional equations for the conservation of momentum in the axial and radial directions are given by the following:

$$M_x: \qquad \rho\left(V_r\frac{\partial V_x}{\partial r}+V_x\frac{\partial V_x}{\partial x}\right)=-\frac{\partial p}{\partial x}+\mu\left[\frac{1}{r}\frac{\partial}{\partial r}\left(r\frac{\partial V_x}{\partial r}\right)+\frac{\partial^2 V_x}{\partial x^2}\right] \tag{1a}$$

$$M_r: \qquad \rho\left(V_r\frac{\partial V_r}{\partial r}+V_x\frac{\partial V_r}{\partial x}\right)=-\frac{\partial p}{\partial r}+\mu\left[\frac{\partial}{\partial r}\left(\frac{1}{r}\frac{\partial}{\partial r}(rV_r)\right)+\frac{\partial^2 V_r}{\partial x^2}\right] \tag{1b}$$

where V_x and V_r are the velocity components in the axial and radial directions, p is the pressure, ρ is the density and μ is the viscosity coefficient, The dimensionless "plus" variables are defined by the following:

$$x^+=\frac{x}{(\mathrm{Re})D},\ r^+=\frac{r}{D},\ \ V_x^+=\frac{V_x}{V_b},\ V_r^+=\frac{V_r(\mathrm{Re})}{V_b},\ p^+=\frac{p}{\rho V_b^2} \tag{2}$$

where D is the pipe diameter and V_b is the bulk (mean) velocity. If the axial diffusion terms in **Eq. (1)** are negligibly small, substitution of **Eq. (2)** into **Eq. (1)** produces the dimensionless momentum equations given by the following:

$$M_x^+: \qquad V_r^+\frac{\partial V_x^+}{\partial r^+}+V_x^+\frac{\partial V_x^+}{\partial x^+}=-\frac{\partial p^+}{\partial x^+}+\frac{1}{r^+}\frac{\partial}{\partial r^+}\left(r^+\frac{\partial V_x^+}{\partial r^+}\right) \tag{3a}$$

$$M_r^+: \qquad V_r^+\frac{\partial V_r^+}{\partial r^+}+\frac{1}{\mathrm{Re}}V_x^+\frac{\partial V_r^+}{\partial x^+}=-\mathrm{Re}\frac{\partial p}{\partial r^+}+\frac{1}{\mathrm{Re}}\left[\frac{\partial}{\partial r^+}\left(\frac{1}{r^+}\frac{\partial}{\partial r^+}(r^+V_r^+)\right)\right] \tag{3b}$$

which shows that the dimensionless axial momentum equation, i.e., **Eq. (3a)**, is independent of the Reynolds number. In the so-called "boundary-layer approximation" that is valid for high Reynolds numbers, **Eq. (3a)** is employed to obtain a numerical or integral method solution, whereas **Eq. (3b)** is ignored. In this study, the dimensional Navier-Stokes equations are solved for various Reynolds numbers from 1 to 2000. If the assumptions of negligibly small radial velocity and axial diffusion ("boundary-layer approximation") are indeed correct, the solutions for different Reynolds numbers are expected to collapse, which is the case for relatively higher Reynolds numbers. At low Reynolds numbers, the axial diffusion and radial

velocity become large, and solutions are expected to show a significant Reynolds number effect.

Momentum and kinetic energy correction factors (β and α, respectively) are useful to compensate for non-uniformity of velocity profiles in engineering calculations and are given by

$$\beta = 2\int_0^1 \left(\frac{V_x}{V_b}\right)^2 \eta d\eta \tag{4a}$$

$$\alpha = 2\int_0^1 \left(\frac{V_x}{V_b}\right)^3 \eta d\eta \tag{4b}$$

where $\eta = r/R$. The fully developed values of β and α are, $\beta_0 = 4/3$ and, $\alpha_0 = 2$, respectively. β and α are both measures of deviation from flow uniformity and are equal to one at the idealized inlet. The momentum correction factor β is related to the pressure drop and the skin-friction coefficient, as shown in Appendix A to be discussed in Section 4.3.

The current study provides two types of analytic expressions that describe the streamwise development of a given flow variable in a smooth circular pipe flow:

1. First, a mathematical expression is proposed for the streamwise variation of a given flow variable and based on that expression, non-linear regression is applied to the computational data for $200 \leq \mathrm{Re} \leq 2000$ and $x^+ \geq 0.001$. Thus, a set of expression parameters are obtained for the specified range of Reynolds number and streamwise location, which finally yields the **High Reynolds Number Correlation (HRNC)** for that flow variable. It should be noted that an HRNC for a given flow variable has a single set of expression parameters whose Reynolds number dependence is not considered. The idea behind the **HRNC**s is that data collapse on each other for $\mathrm{Re} \geq 200$.

2. Using the same mathematical expression as that of the HRNC for a given flow variable, a more accurate correlation is obtained by a two-stage nonlinear regression, which is valid for all Reynolds numbers between 1 and 2000, and $x^+ \geq 0.001$. Here, Reynolds number dependence of the expression parameters is considered. For this purpose, **First Stage Nonlinear Regression (FSNR)** is applied to the computational data for each Reynolds number considered; that is, Reynolds numbers of 1, 2, 3, 4, 6, 8, 10, 16, 20, 25, 30, 36, 40, 50, 70, 100, 140, 200, 250, 300, 500, 700, 1000, 1500 and 2000; and a set of expression parameters corresponding to each Reynolds number are obtained. The process of determining the expression parameters is repeated for each Reynolds number by applying the **FSNR**. Then, **Second Stage Nonlinear Regression (SSNR)** is applied to find the variation of these expression parameters with the Reynolds number. This procedure is like that of **Weigand and Abdelmoula [27]** who employed linear regression analysis to obtain correlations for the Nusselt number in the extended Graetz problem, which considers axial heat conduction in laminar duct flow. The general correlations obtained by two-stage nonlinear regression here are more accurate than **HRNC**s.

The correlations given here apply to flows with heat transfer as well, under the assumptions of constant property and negligible buoyancy for which the velocity field is independent of the temperature field. These assumptions may not be valid in some real-life flows especially at low Reynolds numbers. Experimental results of **Tam and Ghajar [26]** indicate that the friction factor increases with increasing wall heating due to secondary flows induced by buoyancy.

The correlations proposed in this paper are based on solutions of the Navier-Stokes equations (**Eqs. 1a** and **1b**). **Equations 3a** and **3b** are presented to show that solutions for high

Reynolds numbers become independent of the Reynolds number. This also provides a theoretical basis for the validity of our **High Reynolds Number Correlations.**

3. VERIFICATION AND VALIDATION

Axisymmetric laminar flow calculations are conducted using the *ANSYS Fluent* solver, which employs the finite volume method for the discretization of the governing equations. The incompressible steady Navier-Stokes equations are solved with no-slip boundary condition on the wall. A rectangular domain is created representing only half of the circular pipe cross-section where the top and bottom boundaries are defined as wall and axis, while the upstream and downstream boundaries are velocity inlet and outflow (velocity is independent of streamwise distance), respectively (**Fig. 1**)**.** The pipe diameter is D = 0.001 m for all cases, while the pipe length, L, is not constant and is adjusted according to the corresponding Reynolds number, so that $L/D(\mathrm{Re}) = 1$. For instance, for the Reynolds number of Re = 100, the pipe length is L = 0.1 m. The pipe inlet is ideal, i.e., a uniform velocity profile is specified at the inlet. It is assumed that the pipe walls are smooth, that is, the height of the surface roughness is several orders of magnitude smaller than the laminar boundary layer thickness everywhere in the domain.

To accelerate convergence, the coupled algorithm is employed which solves the continuity and momentum equations simultaneously. Mass fluxes on cell faces are obtained using the Rhie-Chow interpolation scheme **[28]**. Second-order upwind interpolation is used for discretization of the convective terms in the momentum equations, while the diffusive terms are discretized by central differencing. Second order interpolation is adopted for pressure.

A mesh independence study is conducted to guarantee that there is no effect of mesh size on the calculated flow field. The data range considered in this study covers the region of $x^+ \geq 0.001$, and therefore, to achieve mesh independence, care has been taken for the invariance of

183 the values of field variables at x^+ = 0.001, and beyond. Accordingly, computations are
184 performed by employing structured meshes of all-rectangular elements such that the
185 streamwise grid spacing near the pipe inlet ($0 \leq x^+ \leq 0.1$) is in the order of $x^+ = 10^{-4}$ at most,
186 resulting in element counts ranging from approximately 2.5x10^5 to 8.5x10^6, while smaller
187 elements are created near the wall, as well **(Fig. 2)**. Δr^+ mesh spacing values in the radial
188 direction next to the wall vary between 2.7×10^{-3} and 2.7×10^{-4}. The Grid Convergence Index
189 (GCI) methodology proposed by **Roache [29]** is adopted to evaluate the mesh independence
190 of the calculated flow field. For this purpose, values of the normalized local skin friction
191 coefficient (c_f/c_{f0}) at the streamwise location of x^+ = 0.005 are compared for a coarse and a
192 fine grid, as the Reynolds number is Re = 1. Accordingly, the lower and upper bounds of
193 c_f/c_{f0} differ less than 0.004%, therefore, sizing configuration of the fine grid is employed in
194 the numerical calculations **(Table 1)**.

195 Validation of the solution procedure is performed by comparing the calculated velocity
196 profiles in the fully developed flow region (at x^+= 0.1) with the well-known parabolic
197 velocity profile, as shown in **Fig. 3**. Comparison of the numerical and theoretical values of
198 velocity indicates that the accuracy of the calculations is better than 99%.

199 **4. RESULTS**

200 In this section, mathematical expressions for streamwise variation of dimensionless variables
201 such as the centerline velocity ($V_c^+ = V_c/V_b$), the normalized local skin friction coefficient
202 (c_f/c_{f0}) and the dimensionless pressure drop (σ); as well as that of the momentum and kinetic
203 energy flux correction factors (β and α) are presented, which are valid for the range of 1 ≤ Re
204 ≤ 2000 and $x^+ \geq 0.001$. These expressions are obtained by application of nonlinear
205 regression on the computational data for each Reynolds number. Streamwise variation of the
206 variables considered here can mathematically be expressed by equations with up to five

parameters where values of expression parameters vary with the Reynolds number. Therefore, a second stage of nonlinear regression is conducted to obtain the Reynolds number dependence of the expression parameters, while peak and sigmoid functions are common to the expression parameter set of a particular flow variable. The Reynolds-number-dependent expressions presented for the streamwise development of the flow variables estimate the data with a maximum **Normalized Root Mean Square Error (NRMSE)** less than 3%. Results for high Reynolds numbers (within the range of $200 \leq \mathrm{Re} \leq 2000$ and $x^+ \geq 0.001$) can be represented by expressions containing constant parameters which are called **High Reynolds Number Correlations (HRNC)**, with an **NRMSE** less than 4%. **HRNC** are simple because they do not contain any parameters describing Reynolds number dependence. However, the expressions that include Reynolds number dependent parameters are more accurate and valid in a larger Reynolds number range between 1 and 2000. Mathematical expressions proposed in this study have been chosen by a trial-and-error procedure that aimed at maximum accuracy and minimum number of correlation parameters. All expressions proposed in the paper are original, i.e., they are not modified versions of any previously reported correlations.

The correlations proposed in this study are valid for idealized inlet conditions, which are not so uncommon and difficult to obtain in practice. For inlets with sharp corners, existing data in the literature suggest that the solution quickly relaxes back to the ideal inlet solution **[11]**. Thus, correlations of this paper are expected to be valid even for sharp inlets for large x^+. Bell-mouth entry and rounding of a sharp inlet with a large radius (compared to pipe radius) causes boundary-layer formation on a curved surface of unspecified length. However, a rounded corner inlet with a small radius would produce almost uniform flow conditions at the inlet.

4.1. Velocity Field

Results for the developing velocity field are presented in this section. **Figure 4** shows the normalized axial velocity profiles $V_x^+ = V_x/V_b$ at $x^+ = 0.005$ for various values of the Reynolds number. The observed concavity of the profiles (velocity overshoot, velocity profile inversion) is well-known and reported for example in **Durst et al. [20]**, **Reci et al. [21],** and **Shah and Bhatti [25]**. It can be hypothesized that relatively larger momentum diffusion at smaller Reynolds numbers generates a thicker boundary-layer at the pipe inlet. The response of the inviscid core is to accelerate to overshoot velocities to satisfy the conservation of mass. In **Fig. 4,** axial velocity profiles of this study are compared with those of numerical solutions of the Navier-Stokes equations obtained by **Haustein and Kashi [11]** and **Shimomukai and Kanda [16]**; as well as **Hornbeck [15]**, who solved the "boundary-layer approximation" equations numerically. The axial velocity profiles obtained from these works all agree very well and differ from the results of this work (for Re = 200 and Re = 2000) by less than 3% as expected in a high Reynolds number flow.

Figure 5 shows the streamwise variation of dimensionless axial centerline velocity profiles ($V_c^+ = V_c/V_b$) and reveals the Re number dependence of development for small x^+ values. Results of the numerical solutions obtained by **Friedmann et al. [17]** and **Shimomukai and Kanda [16]**; as well as the analytical solutions by **Fargie and Martin [10]**, and **Hornbeck [15]** are included in **Fig. 5**. The dimensionless centerline velocity reaches 99% of its fully developed flow value of $V_c^+ = 2$ between $0.05 < x^+ < 0.06$, for Re ≥ 50, which is consistent with the well-known entrance-length of $L_e^+ = 0.06$ **[15, 18, 20]**. The proposed expression for streamwise variation of V_c^+ is given by **Eq. (5)**:

$$V_c^+ = 2 - \frac{1}{[1 + (ax^+)^b]^c} \tag{5}$$

Parameters of **HRNC** for V_c^+ are calculated as a = 1.167, b = 0.872, and c = 40.329, using the mathematical model given by **Eq. (5)**; where data collapse approximately onto a single curve (labeled as **HRNC** in **Fig. 5**) with an **NRMSE** less than 3% within the specified range. The HRNC for V_c^+ is given by **Eq. (6)**:

$$V_c^+ = 2 - \frac{1}{[1 + (1.167x^+)^{0.872}]^{40.329}} \tag{6}$$

Figure 5 shows that our data agree well with the Navier-Stokes solutions of **Shimomukai and Kanda [16]** at Re = 2000, **Friedmann et al. [17**] at Re = 200, and **Haustein and Kashi [11]** at Re = 100. Agreement between our data with the boundary-layer solution of **Hornbeck [15]** and momentum integral solution of **Fargie and Martin [10]** is also reasonably good for large Reynolds numbers (Re > 200) and x^+ values greater than 0.01. The boundary-layer solution of **Hornbeck [15]** and momentum integral solution of **Fargie and Martin [10]** employ some assumptions for the Navier-Stokes equations, which are invalid for relatively lower Reynolds numbers; and therefore, their data agree with our data only for larger Reynolds numbers. Note that **Eq. (5)** satisfies the condition such that $V_c^+ = 1$ at $x^+ = 0$ at the pipe inlet, where the centerline velocity is equal to the inlet bulk velocity.

The application of the **First Stage Nonlinear Regression (FSNR)** to the computational data yields the fitting parameters a, b, and c for each Reynolds number, which are shown by square symbols in **Fig. 6**. The functional forms of their variation with the Reynolds number are those of a peak function with a plateau for a, as well as an inverse-sigmoid and a sigmoid function for b and c, respectively. Applying **Second Stage Nonlinear Regression (SSNR)** to a-b-c data yields **Eqs. (7a), (7b)** and **(7c)**, respectively, which are plotted as continuous curves in **Figs. 6**. **Equations (7)** estimate the parameters a, b, and c with an **NRMSE** less than 1%; while the maximum overall **NRMSE** in $V_c^+$is less than 3%.

$$a = 0.5\left[\left(1+\tanh\left(0.05(50-\mathrm{Re})\right)\right)\left(96.096-24.454e^{-0.118\mathrm{Re}}-72.422e^{-0.014\mathrm{Re}}\right)\right.$$
$$\left.+\left(1+\tanh\left(0.05(\mathrm{Re}-50)\right)\right)\left(1.009+\frac{59.111}{1+\left(\frac{\mathrm{Re}}{143.817}\right)^{4.090}}\right)\right] \quad (7a)$$

$$b = 0.794+\frac{1.508}{1+\left(\frac{\mathrm{Re}}{74.553}\right)^{1.577}} \quad (7b)$$

$$c = 1.526+\frac{34.121}{1+\left(\frac{\mathrm{Re}}{307.595}\right)^{-3.610}} \quad (7c)$$

4.2. Skin-friction Coefficient

Results for the skin-friction coefficient (Fanning friction factor) $c_f = \mu\frac{\left(-\frac{\partial V_x}{\partial r}\right)_w}{0.5\rho V_b^2}$ are presented in this section. **Figure 7** shows the streamwise variation of the normalized local friction coefficient (c_f/c_{f0}), where c_{f0} is the fully developed value equal to 16/Re. (c_f/c_{f0} is equal to f/f_0 where *f* is the Darcy friction factor and f_0 is the fully developed value of 64/Re). A similar approach for c_f/c_{f0} as that adopted for $V_c^+$is taken to obtain the **HRNC**, and Reynolds number dependence of expression parameters. The proposed expression for axial variation of c_f/c_{f0} is given by **Eq. (8)**:

$$\frac{C_f}{C_{f0}} = 1+\frac{a}{b+\sinh(cx^+)} \quad (8)$$

Parameters for **HRNC** are obtained as *a* = 0.135, *b* = 0.036, and *c* = 56.405, as **HRNC** agrees with the computational data with an **NRMSE** less than 4%. The HRNC for c_f/c_{f0} is given by **Eq. (9)** below:

$$\frac{C_f}{C_{f0}} = 1+\frac{0.135}{0.036+sinh(56.405x^+)} \quad (9)$$

In **Fig. 7**, **HRNC** data for c_f/c_{f0} along with the momentum integral solution of **Fargie and Martin [10]** are presented. The agreement between our Re = 2000 data and the data of **Fargie and Martin [10]** is good, especially for $x^+ > 0.01$.

The Reynolds number dependence of *a*, *b*, and *c* is shown by square symbols in **Fig. 8**. The variation of these parameters with Re is estimated by **Eqs. (10),** which are obtained by a second stage of nonlinear regression and plotted as curves in **Fig. 8**, in the form of inverse sigmoid and peak functions. Parameters *a* and *c* approach a constant value beyond Re = 200, while *b* is the "compensatory" parameter for the slight variation of c_f/c_{f0} for Re ≥ 200. **NRMSE** in the estimation of the parameters *a*, *b*, and *c*; as well as that in c_f/c_{f0} is less than 1%, which indicates the improved accuracy of the so-called two-stage nonlinear regression method.

$$a = 0.13 + 1.00e^{-\mathrm{Re}/2.55} + 4.32e^{-\mathrm{Re}/23.13} \tag{10a}$$

$$b = 0.5\left[\left(1+\tanh\left(0.05(36-\mathrm{Re})\right)\right)\left(-0.015+0.017e^{-\frac{\mathrm{Re}}{70.65}}\sin\left(\pi\frac{\mathrm{Re}+34.31}{53.74}\right)\right) + \left(1+\tanh\left(0.05(\mathrm{Re}-36)\right)\right)(0.052-0.084\times 0.996^{\mathrm{Re}})\right] \tag{10b}$$

$$c = 0.5\left[\left(1+\tanh\left(0.05(30-\mathrm{Re})\right)\right)(207.360-214.208\times 0.919^{\mathrm{Re}}) + \left(1+\tanh\left(0.05(\mathrm{Re}-30)\right)\right)\left(52.635+\frac{123.919}{1+(\mathrm{Re}/61.090)^{3.574}}\right)\right] \tag{10c}$$

4.3. Dimensionless Pressure Drop

Figure 9 shows the streamwise variation of the dimensionless pressure drop $\sigma = (P_i - P)/(0.5\rho V_b^2)$ where P_i and *P* are the inlet and local pressures, respectively, both on the centerline. The centerline pressure P_i was preferred over an area averaged sectional pressure in the definition of σ, because P_i is easier to determine experimentally. The pressure drop data collapse onto a single curve for a relatively larger range of Reynolds number, i. e., for 200 ≤ Re ≤ 2000, and can be conveniently estimated using **Eq. (11)** which has a quite simple

303 form, and is valid for $x^+ \geq 0.001$ with a maximum **NRMSE** less than 2%. An expression
304 reported by **Shah and London [1]** (Eq. 191) is also plotted for comparison, which slightly
305 overestimates our σ data with a maximum **NRMSE** around 2%. **Equation (11)** is the **HRNC**
306 for σ and given as follows:

$$\sigma = 0.916 + 64(x^+) \tag{11}$$

307 Appendix A presents a relationship **(Eq. A2)** between pressure drop, σ, Fanning friction
308 factor C_f, and momentum correction factor β; and shows that the pressure drop has two
309 components: $\sigma_m = 2(\beta - 1)$ is the momentum flux component and σ_f is the friction
310 component. σ_m increases along the streamwise direction and reaches a maximum value of
311 0.66 in the fully developed flow region. For high Reynolds numbers, streamwise variation of
312 C_f is negligibly small. Assuming a constant value of 16/Re for C_f, σ_f is evaluated as $64(x^+)$.
313 Also, for high Reynolds numbers, contribution of the exponential terms in **Eqs. (A3)** and **(A4)**
314 are negligibly small so that a simple correlation in the form of **Eq. (11)** becomes sufficiently
315 accurate.

316 Rearrangement of **Eq. (11)** yields the dimensionless pressure difference, Δp^+, between any
317 two locations x_1^+ and x_2^+ on the centerline, which is defined as, $\Delta p^+ = (P_1 - P_2)/(0.5\rho V_b^2)$
318 and given by **Eq. (12)** that is valid for 200 ≤ Re ≤ 2000:

$$\Delta p^+ = 64[(x_2^+) - (x_1^+)] \tag{12}$$

319 It is interesting to note the region of negative σ in **Fig. 9**, which is more pronounced for
320 relatively smaller Re, indicating an increase in pressure in the streamwise direction; and
321 extending approximately up to $x^+ = 0.3$ for Re = 1, and $x^+ = 0.06$ for Re = 4, finally
322 diminishing for Re ≥ 50. A negative pressure drop is related to the velocity overshoot, which
323 is accompanied by radial pressure variations near the inlet.

Equation (13) represents the σ data for the whole range of Reynolds numbers, i. e., $1 \leq \mathrm{Re} \leq 2000$, and can estimate σ with a maximum **NRMSE** less than 1%:

$$\sigma = a(x^+)^{(bx^{-c})} + gx^+e^{(-hx^+)}\sin\big(\pi(x^+ - 0.5)\big)\left(\frac{2}{0.5 + e^{x^+}}\right) \tag{13}$$

Equation (13) is a superposition of two functions: The first function (containing the parameters *a*, *b*, and *c*) represents the data for relatively larger Reynolds numbers; whereas the second function (containing the parameters *g*, and *h*) is a combination of exponential and sinusoidal functions and can estimate low Reynolds number data with undershoot. The term $2/\big(0.5 + e^{x^+}\big)$ provides a smooth transition to the first function at larger x^+ values, for all Reynolds numbers; while the parameter *g* becomes zero at high Reynolds numbers (**Fig. 10d**), leading the second function to eventually vanish.

Application of **SSNR** to the σ parameters *a*, *b*, *c*, *g,* and *h* yields **Eq. (14)**, while variations of these parameters with the Reynolds number are illustrated in **Fig. 10**.

$$a = 65.575 - \frac{239.733}{1 + \left(\frac{\mathrm{Re}}{0.111}\right)} \tag{14a}$$

$$b = 0.5\Bigg[\big(1 + \tanh\big(0.05(6 - \mathrm{Re})\big)\big)(0.902 + 0.731e^{-1.211\mathrm{Re}}) + \big(1 + \tanh\big(0.05(\mathrm{Re} - 6)\big)\big)\left(1.012 + \frac{3.856}{1 + \left(\frac{\mathrm{Re}}{0.832}\right)^{3.185}}\right)\Bigg] \tag{14b}$$

$$c = -0.036 + \frac{0.424}{1 + \left(\frac{\mathrm{Re}}{2.816}\right)^{1.175}} \tag{14c}$$

$$g = -0.136 + \frac{76.039}{1 + \left(\frac{\mathrm{Re}}{1.551}\right)^{1.993}} \tag{14d}$$

$$h = 1.833 + \frac{30.924}{\left(1 + \left(\frac{\mathrm{Re}}{11.197}\right)^{-4.077}\right)^{0.298}} \tag{14e}$$

335 **4.4. Integral Parameters**

336 The correction factors of momentum flux, β, and kinetic energy flux, α, are defined by **Eq.**
337 **(4)**, which have fully developed values of β_0 = 1.33 and, $\alpha_0 = 2.00$, respectively. The
338 streamwise development of β and α can be estimated by an exponential decay function, which
339 is given by **Eqs. (15a)** and **(15b)**. Note that parameters a and b take different values for β and
340 α.

$$\beta = \beta_0 - e^{-\left(a(x^+)^b + 1.109\right)} \tag{15a}$$

$$\alpha = \alpha_0 - e^{-\left(a(x^+)^b\right)} \tag{15b}$$

341 Streamwise development of β and α for various Reynolds numbers, as well as the
342 corresponding **HRNC**s, are presented in **Figs. 11** and **12**, respectively. The maximum
343 **NRMSE** in estimation of β and α is less than 3% and 2%, respectively. Parameters for
344 **HRNC** are obtained as a = 24.243, and b = 0.639 for;β and a = 24.582 and b = 0.680 for α,
345 again with a maximum **NRMSE** less than 3% and 2%, respectively. The **HRNC**s for β and α
346 are given by **Eqs. (16a-b)**:

$$\beta = 1.33 - e^{-\left(24.243(x^+)^{0.639} + 1.109\right)} \tag{16a}$$

$$\alpha = 2.00 - e^{-\left(24.582(x^+)^{0.680}\right)} \tag{16b}$$

347 **Equations** (**16a)** and **(16b)** are consistent with the uniform velocity boundary condition at the
348 inlet where both β and α become equal to unity. **Figures 11** and **12** show that values of β and
349 α depart from one (i.e., the incoming flow loses its uniformity) at $x^+ = x/D(\mathrm{Re})$ values as low
350 as 0.001, for all Reynolds numbers. However, departure from velocity uniformity occurs at
351 smaller x/D values for smaller Reynolds numbers due to larger viscous diffusion.

352 **Equations (17)** and **(18)** are obtained by applying nonlinear regression to expression
353 parameters of β and α, which are plotted in **Figs. 13** and **14**, respectively. **NRMSE** in the
354 estimation of the parameters a and b is less than 1%. The functional forms of corresponding

355 expression parameters are the same, where a peak function with a plateau and an inverse
356 sigmoid function are obtained for a and b, respectively. Asymptotic behavior of parameters a
357 and b is evident for Re ≥ 200. Thus, the parameters a and b for the momentum flux correction
358 factor β in **Eq. (15a)** are given by

$$a = 0.5\left[\left(1+\tanh\left(0.05(16-\mathrm{Re})\right)\right)\left(148.904-\frac{259.790}{1+e^{\left(\frac{\mathrm{Re}-3.300}{4.417}\right)}}\right) + \left(1+\tanh\left(0.05(\mathrm{Re}-16)\right)\right)\left(23.610+85.498e^{\left(-\frac{\mathrm{Re}}{57.134}\right)}\right)\right] \tag{17a}$$

$$b = 0.609+\frac{0.831}{1+\left(\frac{\mathrm{Re}}{31.030}\right)^{1.269}} \tag{17b}$$

359 The parameters a and b for the kinetic energy flux correction factor α in **Eq. (15b)** are given
360 by

$$a = 0.5\left[\left(1+\tanh\left(0.05(16-\mathrm{Re})\right)\right)\left(164.519-\frac{266.815}{1+e^{\left(\frac{\mathrm{Re}-3.685}{4.005}\right)}}\right) + \left(1+\tanh\left(0.05(\mathrm{Re}-16)\right)\right)\left(24.060+72.323e^{\left(-\frac{\mathrm{Re}}{60.247}\right)}\right)\right] \tag{18a}$$

$$b = 0.653+\frac{0.880}{1+\left(\frac{\mathrm{Re}}{28.087}\right)^{1.281}} \tag{18b}$$

361 ## 5. SUMMARY and CONCLUSIONS

362 Numerical solutions of the incompressible steady Navier-Stokes equations for laminar
363 circular pipe flow in the region of hydrodynamic development with uniform inlet velocity
364 profile are presented. Mathematical expressions for streamwise variation of the centerline
365 velocity, the normalized local skin friction coefficient and the dimensionless pressure drop; as
366 well as integral parameters such as the momentum and kinetic energy flux correction factors,
367 are obtained by applying a two-stage nonlinear regression on the computational data for
368 Reynolds numbers from 1 to 2000, and $x^+ \geq 0.001$. Since values of expression parameters
369 vary with the Reynolds number, a second stage of nonlinear regression is conducted to obtain

their variation with the Reynolds number, which can be represented by a peak function with a plateau and sigmoid and inverse sigmoid functions. The analytic expressions for the streamwise development of the flow variables obtained by two-stage regression contain parameters, which depend on the Reynolds number and estimate the data with a maximum **NRMSE** of less than 3%.

Also, **High Reynolds Number Correlations (HRNC)**, containing constant expression parameters, are provided for each variable, which are valid within the range of 200 ≤ Re ≤ 2000 and, $x^+ \geq 0.001$ with an **NRMSE** less than 4%. The **HRNCs** for the variables considered in this study can be summarized as follows:

$$V_c^+ = 2 - \frac{1}{[1 + (1.167x^+)^{0.872}]^{40.329}}$$

$$\frac{C_f}{C_{f0}} = 1 + \frac{0.135}{0.036 + \sinh(56.405x^+)}$$

$$\sigma = 0.916 + 64(x^+)$$

$$\beta = 1.33 - e^{-\left(24.243(x^+)^{0.639} + 1.109\right)}$$

$$\alpha = 2.00 - e^{-\left(24.582(x^+)^{0.680}\right)}$$

Comparison of our data with previous studies shows that the boundary-layer and momentum integral solutions reported in the literature are reasonably accurate for Re > 200 and $x^+ > 0.1$. The analytic equations presented here apply to flows with heat transfer as well, provided that the velocity field can be assumed to be independent of the temperature field. Thus, the proposed correlations may be used in the design of heat exchangers. The expressions presented may also be used for developing flow in noncircular channels by replacing the pipe diameter with the hydraulic diameter in the definitions of the non-dimensional parameters. However, the accuracy of such an approximation requires determination by a new study.

387 Also, the effect of the inlet geometry on the accuracy of the proposed correlations may be
388 studied in a future study.

NOMENCLATURE

c_f skin-friction coefficient $\left(\mu \frac{\left(-\frac{\partial V_x}{\partial r}\right)_w}{0.5\rho V_b^2}\right)$

D pipe diameter, m

f Darcy friction factor $(4c_f)$

p pressure, Pa

R pipe radius, m

Re Reynolds number $\left(\frac{\rho V_b D}{\mu}\right)$

V velocity, m/s

x, r axial and radial coordinates, m

Greek symbols

α kinetic energy correction factor

β momentum correction factor

η normalized radial coordinate $\left(\frac{r}{R}\right)$

μ absolute viscosity, kg/ms

ρ density, kg/m^3

σ dimensionless pressure drop $\left(\frac{p_i - p}{0.5\rho V_b^2}\right)$

Subscripts

b bulk (sectional mean)

c centerline

i inlet

r radial component

x axial component

0 fully developed value

Abbreviations

FSNR	First Stage Nonlinear Regression
GCI	Grid Convergence Index
HRNC	High Reynolds Number Correlations
NRMSE	Normalized Root Mean Square Error
SSNR	Second Stage Nonlinear Regression

REFERENCES

[1] Shah, R.K., and London, A.L., 1978, *Laminar flow forced convection in ducts: a source book for compact heat exchanger analytical data*, Academic Press, New York.

[2] Shah, R.K., 1978, "A correlation for laminar hydrodynamic entry length solutions for circular and noncircular ducts", *J. Fluids Eng.*, 100, 177-179. 10.1115/1.3448626

[3] Li, H., Li, Y. Huang, B., and Xu, T., 2020, "Flow characteristics of the entrance region with roughness effect within rectangular microchannels", *Micromachines*, 11(1), 30-47. 10.3390/mi11010030

[4] Colin, S., 2012, "Gas microflows in the slip flow regime: a critical review on convective heat transfer", *J. Heat Transfer*, 134, 020908 (1–13). 10.1115/1.4005063

[5] Rehman, D. Barattini, D., Hong, C., and Morini, G.L., 2021, "Effect of aspect ratio and inlet manifold shape on the laminar-to-turbulent transition of gas flow in rectangular microchannels", *Exp. Fluids*, 62:52. 10.1007/s00348-021-03137-3

[6] Sharp, K.V., and Adrian, R.J., 2004, "Transition from laminar to turbulent flow in liquid filled microtubes", *Exp. Fluids*, 36, 741-747. 10.1007/s00348-004-0893-0

[7] White, F., 2015, *Fluid Mechanics*, 8th ed., McGraw-Hill, New York.

[8] Elger, D.F., Williams, B.C., Crowe C.T. and Roberson, J.A., 2014, *Engineering Fluid Mechanics*, 10th ed., John Wiley & Sons, New York.

[9] Cengel, Y., Cimbala; J., and Ghajar, A., 2022, *Fundamentals of Thermal-Fluid Sciences*, 6th ed., McGraw-Hill, New York.

[10] Fargie, D., and Martin, B. W., 1971, "Developing laminar flow in a pipe of circular cross section", *Proc. R. Soc. London*, Ser. A, 321, 461–476. 10.1098/rspa.1971.0043

[11] Haustein, H. D., and Kashi, B., 2019, "Distortion of pipe-flow development by boundary layer growth and unconstrained inlet conditions", *Phys. Fluids*, 31(6), 063602, 10.1063/1.5091602

[12] Mohanty, A.K., and Asthana, S.B.L., 1978, "Laminar flow in the entrance region of a smooth pipe", *J. Fluid Mech.*, 90, 433-447. 10.1017/S0022112079002330

[13] Chen, R.Y., 1973, Flow in the entrance region at low Reynolds numbers, J. Fluids Eng., 95, 153-158.

[14] Sparrow, E. M., Lin, S. H., and Lundgren, T. S., 1964, "Flow development in the hydrodynamic entrance region of tubes and ducts", *Phys. Fluids* **7**-3, 338–347. 10.1063/1.1711204

[15] Hornbeck, R. W., 1964, "Laminar flow in the entrance region of a pipe", *Appl. Sci. Res.*, Sect. A, 13, 224–236. 10.1007/BF00382049

[16] Shimomukai, K., and Kanda, H., 2008, "Numerical study of normal pressure distribution in entrance pipe flow", *Electron. Trans. Numer. Anal.*, 30, 10-25.

[17] Friedmann, M., Gillis, J., and Liron, N., 1968, "Laminar Flow in a pipe at low and moderate Reynolds numbers", *Appl. Sci. Res*, 19, 426-438. 10.1007/BF00383937

[18] Dombrowski, N., Foumeny, E.A., Ookawara, S., and Riza, A., 1993, "The influence of Reynolds number on the entry length and pressure drop for laminar flow", *Can. J. Chem. Eng.*, 71, 472-476. 10.1002/cjce.5450710320

[19] Kountouriotis, Z., Philippou, M., and Georgiou, G. C., 2016, "Development lengths in Newtonian Poiseuille flow with wall slip", *Applied Math. Comput.*, 291, 98-114. 10.1016/j.amc.2016.06.041

[20] Durst, F., Ray, S., Ünsal, B., and Bayoumi, O. A., 2005, "The development lengths of laminar pipe and channel flows", *J. Fluids Eng*, 127, 1154-1160. 10.1115/1.2063088.

[21] Reci, A., Sederman, A.J., and Gladden, L.F., 2018, "Experimental evidence of velocity profile inversion in developing laminar flow using magnetic resonance velocimetry", *J. Fluid Mech.*, 851, 545-557. 10.1017/jfm.2018.512

[22] Muzychka, Y. S., and Yovanovich, M. M., 2009, "Pressure drop in laminar developing flow in noncircular ducts: A scaling and modeling approach", *J. Fluids Eng,* 131(11). 111105. 10.1115/1.4000377

[23] Gad-el-Hak, M., 1999, "The Fluid Mechanics of Microdevices - The Freeman Scholar Lecture", *J. Fluids Eng,* 121(11), 5-33. 10.1115/1.2822013

[24] Duan, Z., and Muzychka, Y. S, 2010, "Slip flow in the hydrodynamic entrance region of circular and noncircular microchannels", *J. Fluids Eng*, 132(1). 10.1115/1.4000692

[25] Shah, R. K., and Bhatti, M. S., 1987, "Laminar convective heat transfer in ducts", in *Handbook of Single Phase Convective Heat Transfer*, Chap.3, 137-172, Editors: Kakaç, S, Shah, R.K, and Aung, W., John Wiley & Sons, New York.

[26] Tam, L. M., and Ghajar, A.J., 1997, "Effect of inlet geometry and heating on the fully developed friction factor in the transition region of a horizontal tube", *Exp. Therm. Fluid Sci.*, 15(1), 52-64. 10.1016/S0894-1777(97)00035-6

[27] Weigand, B., and Abdelmoula, M., 2014, "Axial heat conduction effects in the entrance region of laminar duct flows: Correlations for the local Nusselt number", *Int. Commun. Heat Mass Transf.*, 51, 45-50. 10.1016/j.icheatmasstransfer.2014.01.004

[28] Rhie, C. M., and Chow, W. L., 1983, "Numerical study of the turbulent flow past an airfoil with trailing edge separation", *AIAA J.*, 21(11), 1525-1532. 10.2514/3.8284

[29] Roache, P. J., 1994, "Perspective: a method for uniform reporting of grid refinement studies", *J. Fluids Eng.*, 116, 405-413. 10.1115/1.2910291

APPENDIX A

The linear momentum equation written for a cylindrical control volume of radius $R = D/2$ and thickness dx produces a differential expression which is integrated between the pipe inlet and any axial location to obtain the following equation (**Eq. 94** in **Shah and London [1]**):

$$\frac{p_i - p}{\frac{1}{2}\rho V_b^2} = \frac{1}{R}\int_0^x C_f dx + \frac{2}{\pi R^2}\int_0^R \left(\frac{V}{V_b}\right)^2 2\pi r dr - 2 \tag{A.1}$$

Employment of non-dimensional parameters in the above equation gives the following relation between σ, C_f and β:

$$\sigma = 2(\beta - 1) + 4\mathrm{Re}\int_0^{x^+} C_f dx \tag{A.2}$$

The first and second terms on the right-hand side of **Eq. (A.2)** are components of pressure drop due to momentum flux (σ_m) and friction (σ_f), respectively ($\sigma = \sigma_m + \sigma_f$).

The integral in **Eq. (A.2)** can be evaluated analytically if a correlation for C_f is available. Employment of the HRNCs for C_f and β (given by **Eqs. 9** and **16a**) produces

$$\sigma_m = 0.66 - 2e^{-\left[24.453\left(x^+\right)^{0.639} + 1.109\right]} \tag{A.3}$$

$$\sigma_f = 0.62 + 64(x)^+ + 0.15296\ln\frac{e^{56.405x^+} - 0.9646}{e^{56.405x^+} + 1.0366} \tag{A.4}$$

which are valid for $200 \leq \mathrm{Re} \leq 2000$.

FIGURE CAPTIONS

Figure 1. The solution domain with the boundary conditions and geometrical parameters

Figure 2. A view of the numerical grid indicating the distribution of elements near the pipe inlet (the left edge) and the wall (the top edge)

Figure 3. Comparison of calculated and theoretical fully developed velocity profiles

Figure 4. Dimensionless axial velocity V_x^+ profiles at $x^+ = 0.005$

Figure 5. Streamwise variation of the dimensionless axial centerline velocity V_c^+

Figure 6. Variation of V_c^+ parameters *a*, *b*, and *c* with Reynolds number (symbols: **FSNR**, curves: **SSNR**)

Figure 7. Streamwise variation of the local friction coefficient, c_f/c_{f0}

Figure 8. Variation of c_f/c_{f0} parameters *a*, *b*, and *c* with Reynolds number (symbols: **FSNR**, curves: **SSNR**)

Figure 9. Streamwise variation of the dimensionless pressure drop, σ

Figure 10. Variation of σ parameters *a*, *b*, *c*, *g*, and *h* with Reynolds number (symbols: **FSNR**, curves: **SSNR**)

Figure 11. Streamwise variation of the momentum flux correction factor, β

Figure 12. Streamwise variation of the kinetic energy flux correction factor, α

Figure 13. Variation of β parameters *a* and *b* with Reynolds number (symbols: **FSNR**, curves: **SSNR**)

Figure 14. Variations of α parameters *a* and *b* with Reynolds number (symbols: **FSNR**, curves: **SSNR**)

TABLE CAPTIONS

Table 1. Results of the mesh independence study (Re=1)

Figure 1

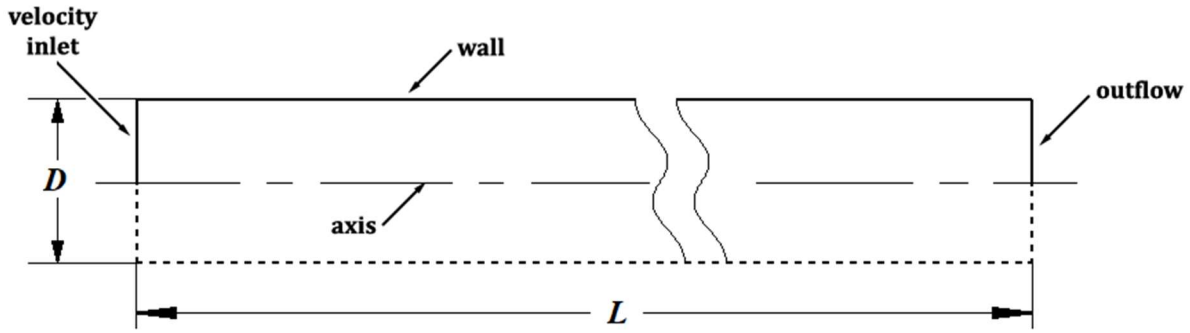

Figure 2

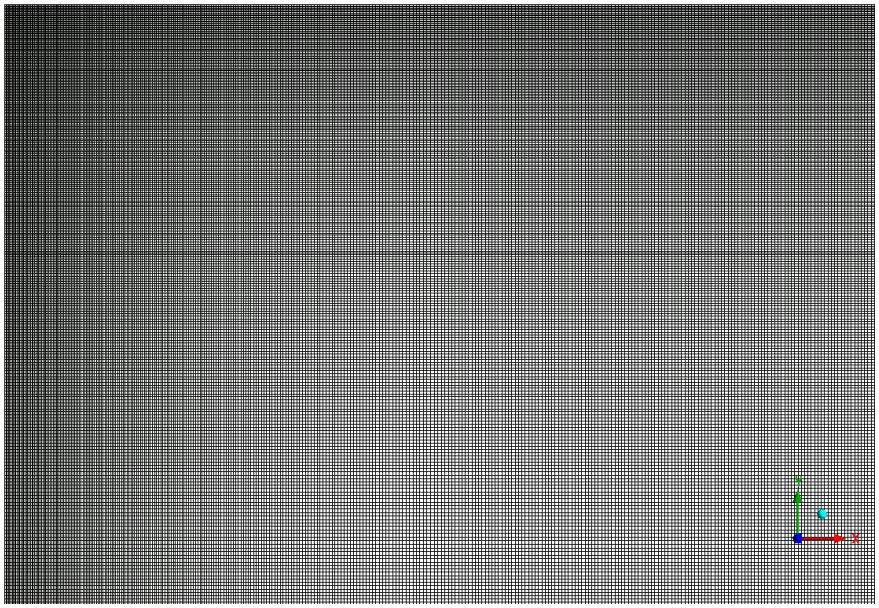

Figure 3

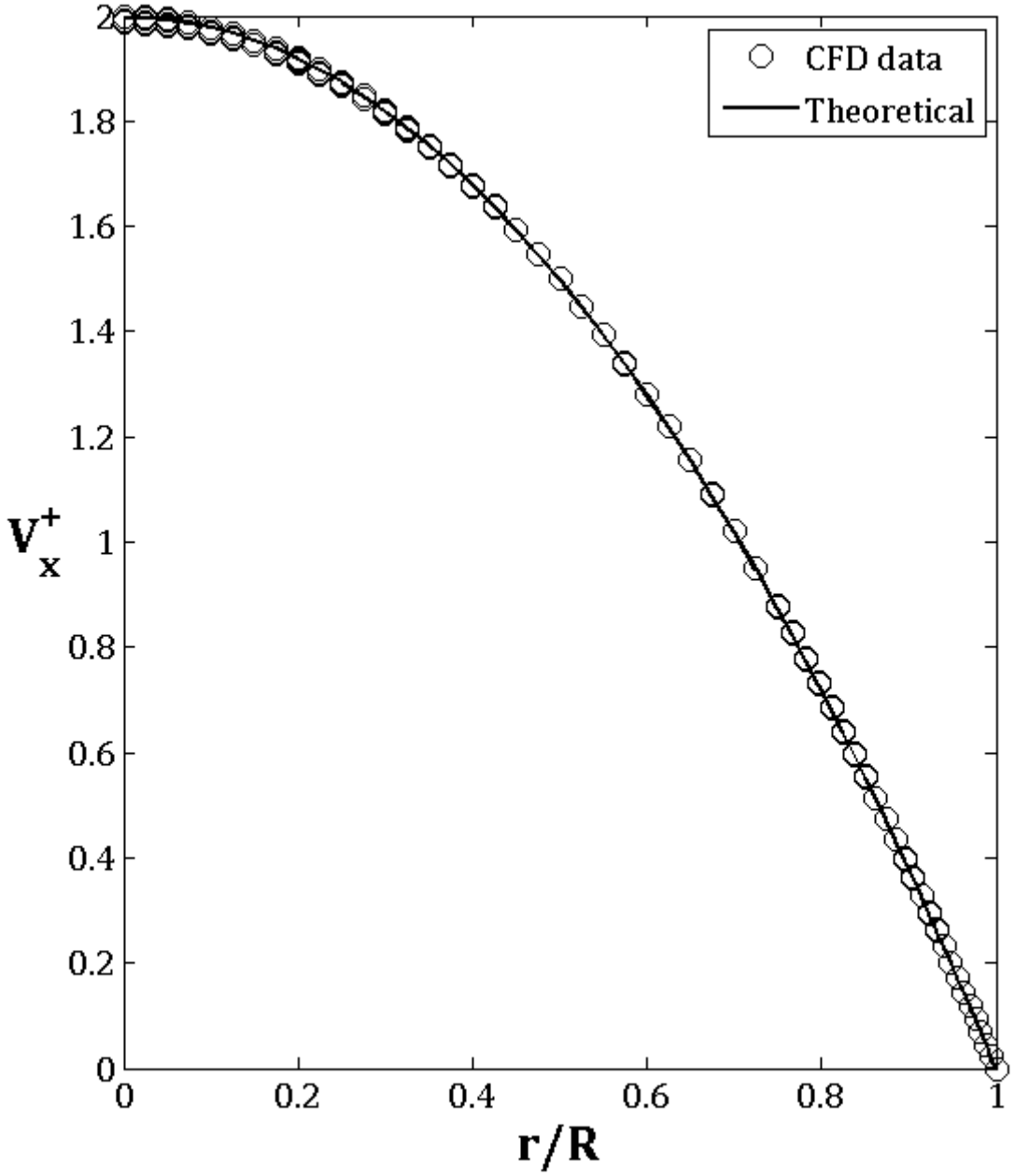

Figure 4

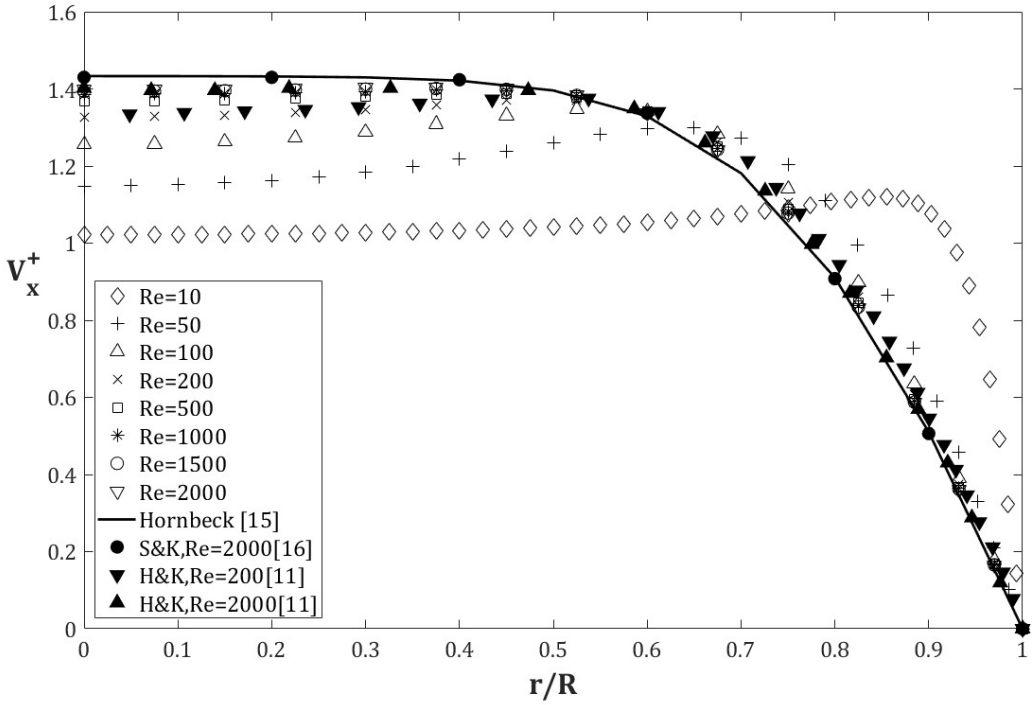
1.6
1.4
1.2
1
0.8
0.6
0.4
0.2
0
V_x^+
0
0.1
0.2
0.3
0.4
0.5
0.6
0.7
0.8
0.9
1
r/R
Re=10
Re=50
Re=100
Re=200
Re=500
Re=1000
Re=1500
Re=2000
Hornbeck [15]
S&K,Re=2000[16]
H&K,Re=200[11]
H&K,Re=2000[11]

Figure 5

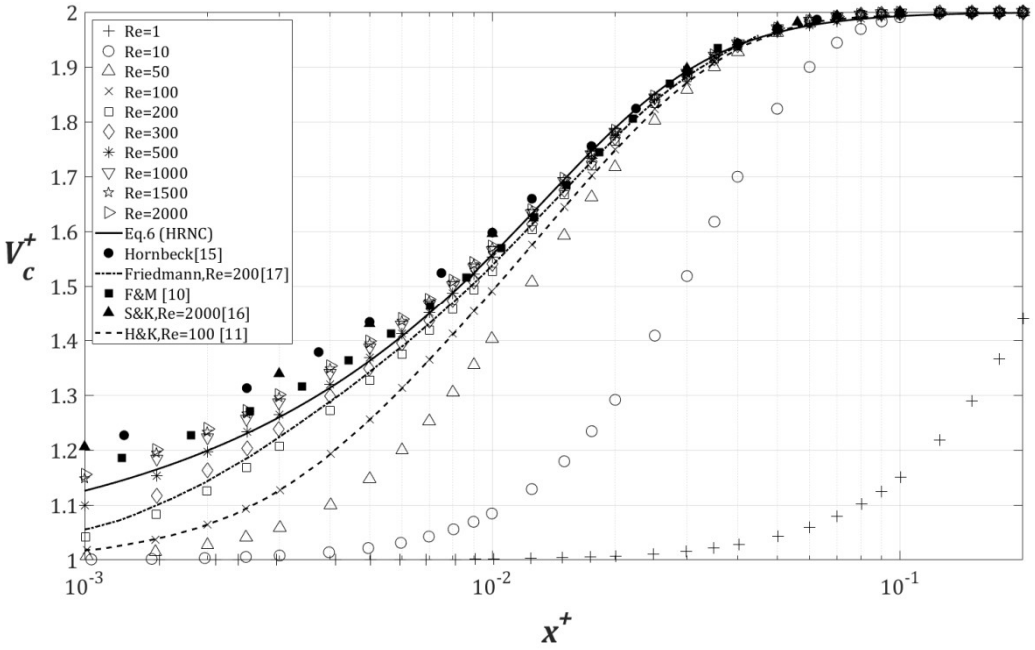
Re=1
Re=10
Re=50
Re=100
Re=200
Re=300
Re=500
Re=1000
Re=1500
Re=2000
Eq.6 (HRNC)
Hornbeck[15]
Friedmann,Re=200[17]
F&M [10]
S&K,Re=2000[16]
H&K,Re=100 [11]
V_c^+
x^+
2
1.9
1.8
1.7
1.6
1.5
1.4
1.3
1.2
1.1
1
10^{-3}
10^{-2}
10^{-1}

Figure 6a

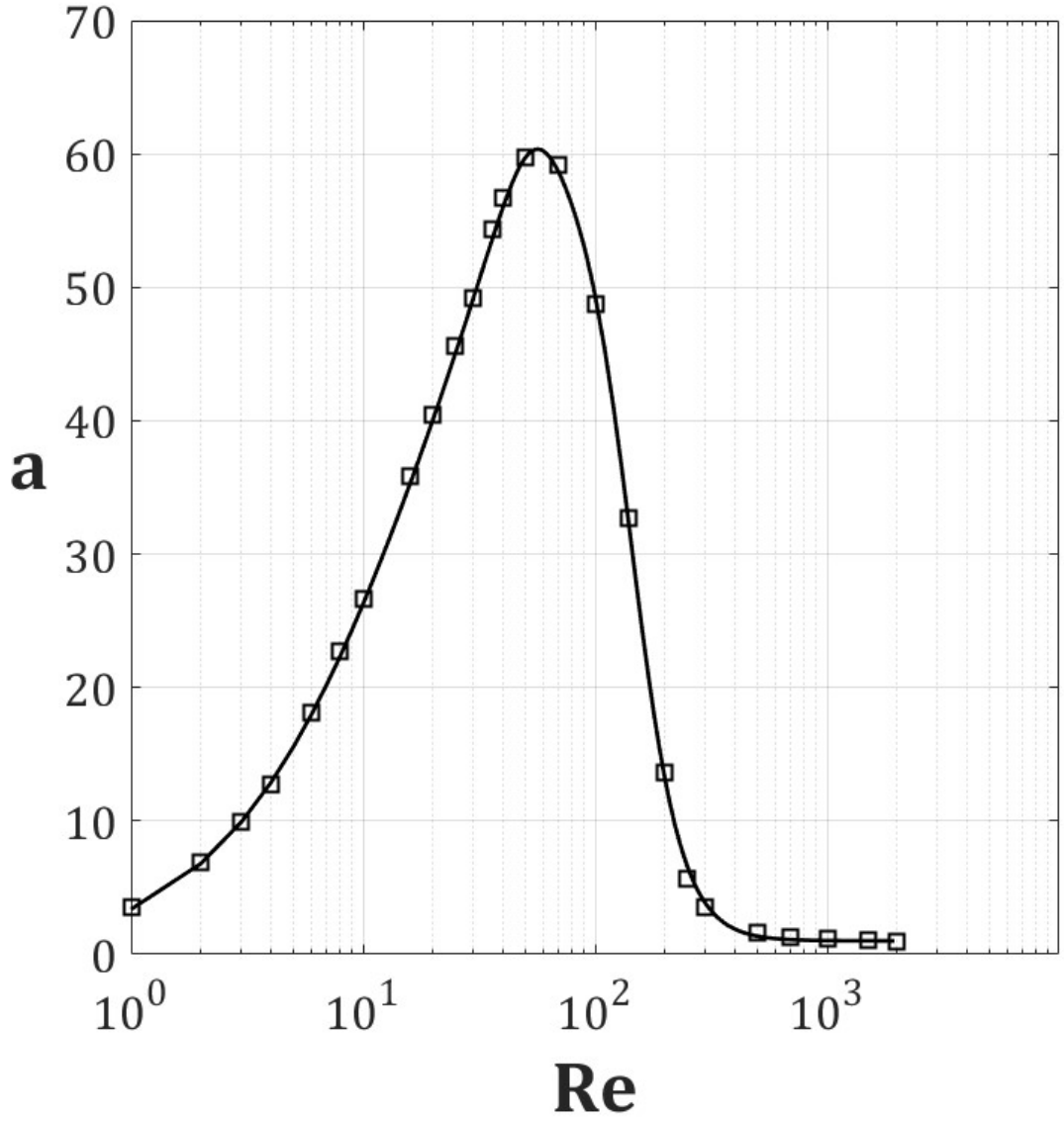

Figure 6b

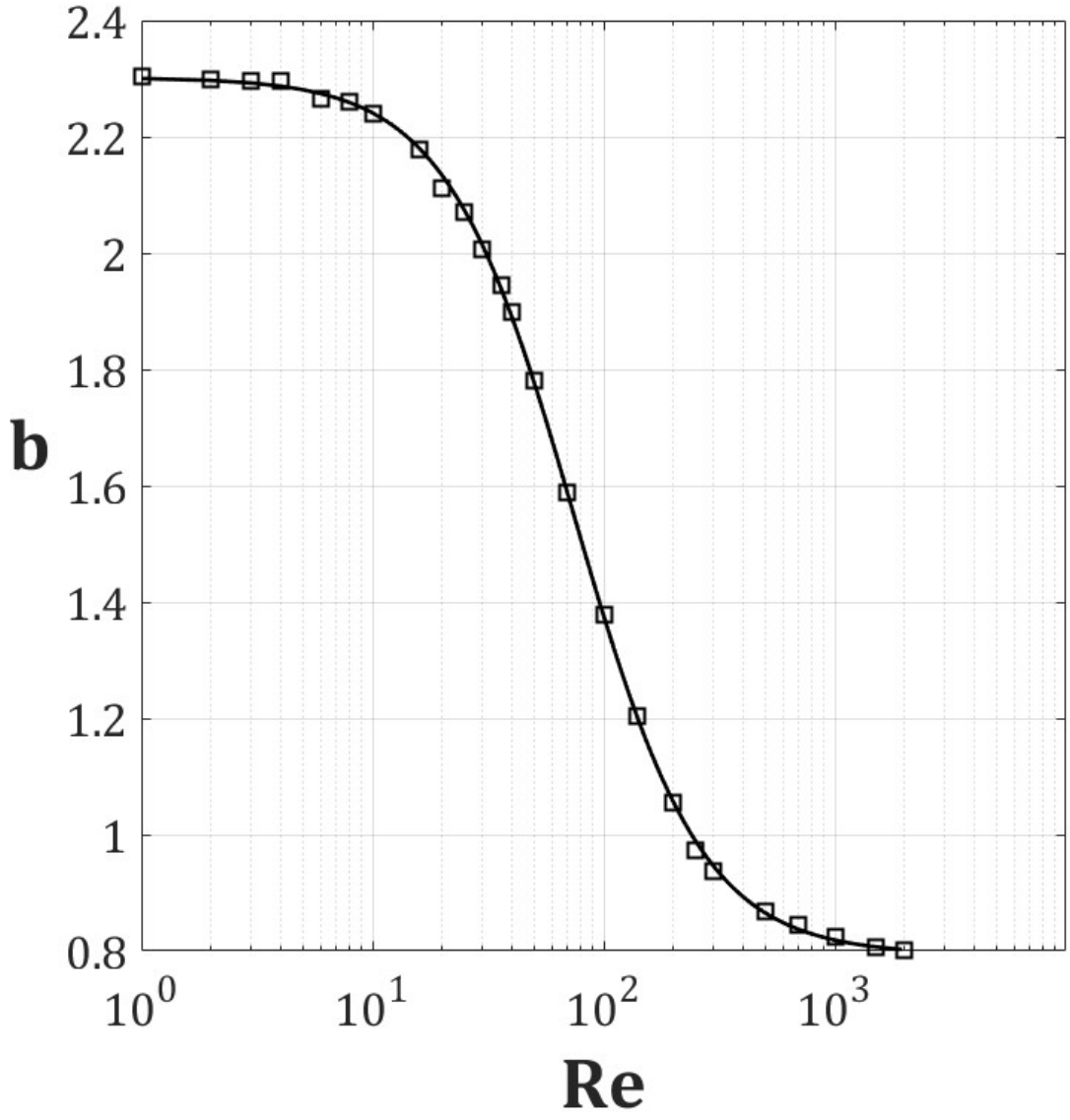

Figure 6c

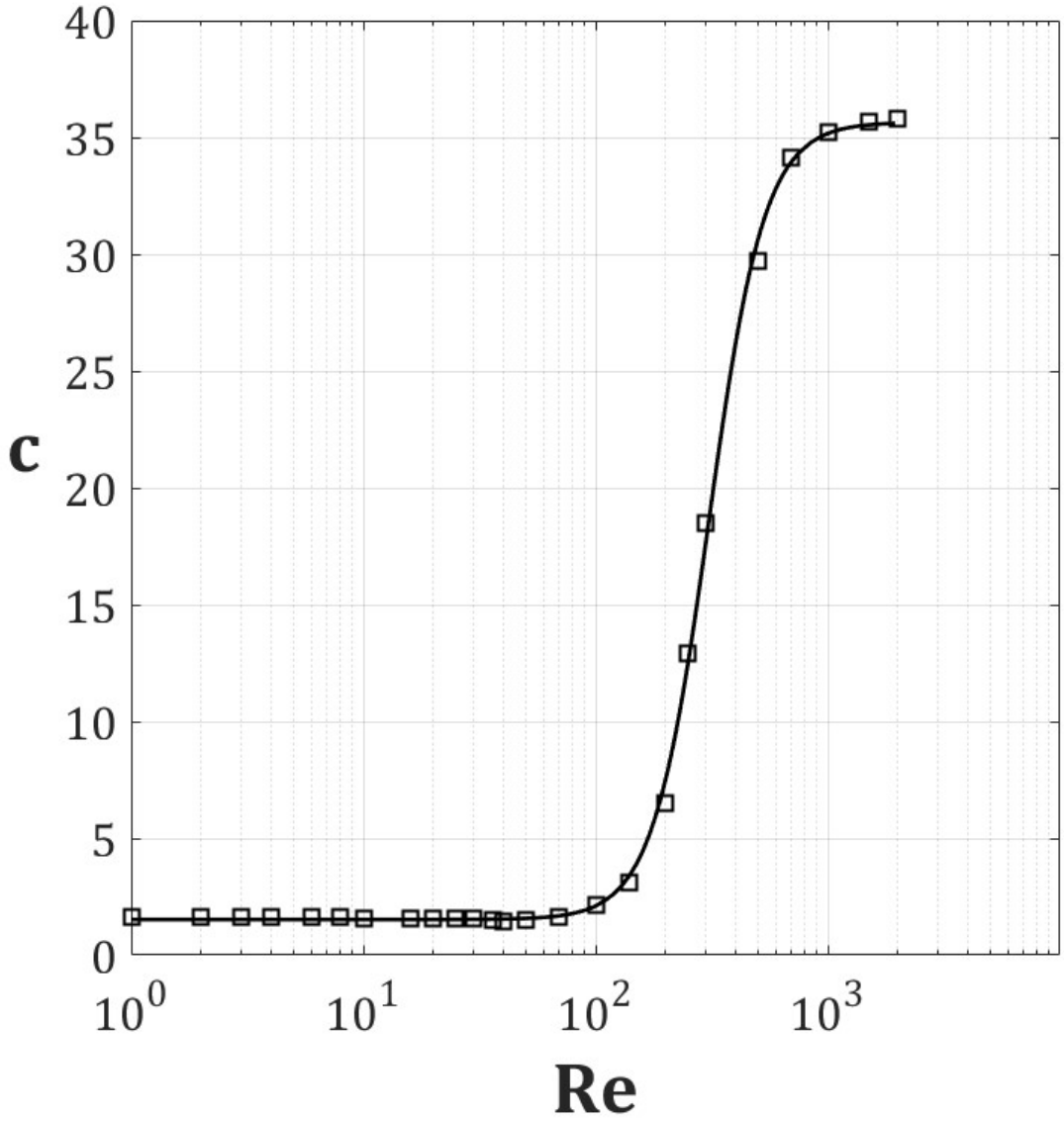

Figure 7

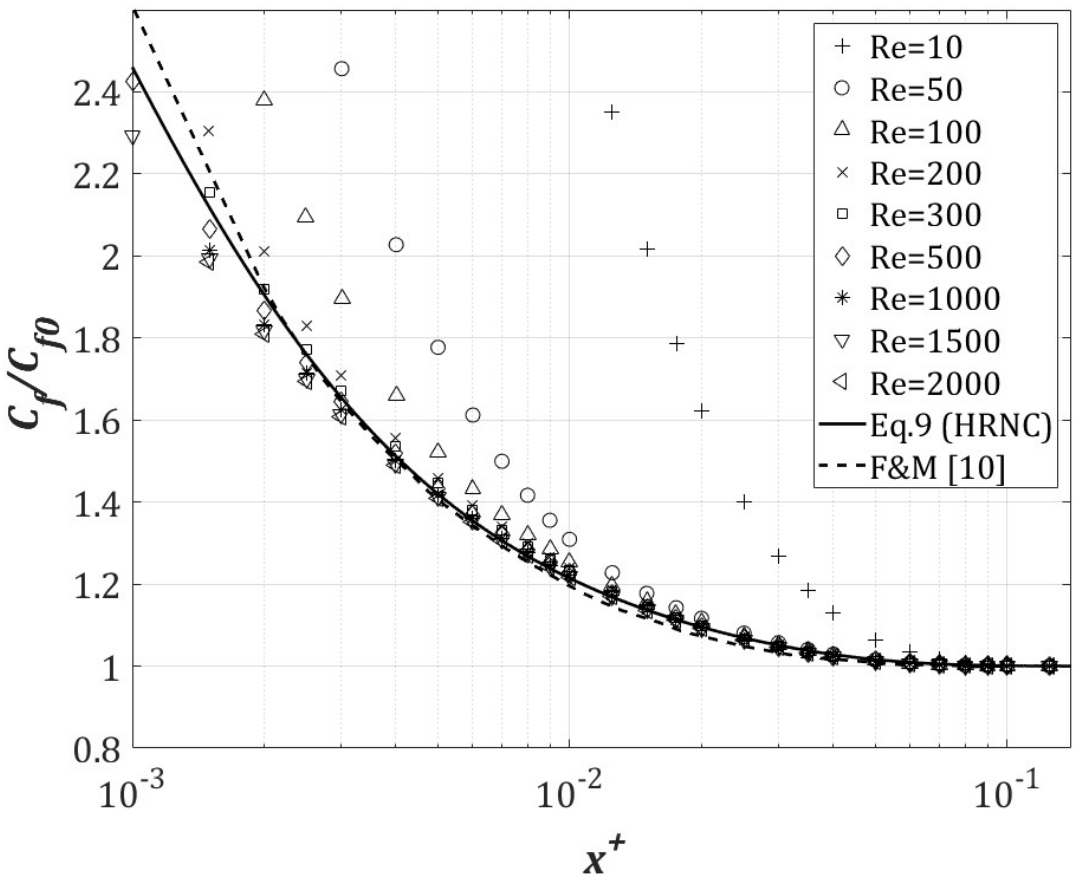
Re=10
Re=50
Re=100
Re=200
Re=300
Re=500
Re=1000
Re=1500
Re=2000
Eq.9 (HRNC)
F&M [10]
C_f/C_{f0}
x^+
2.4
2.2
2
1.8
1.6
1.4
1.2
1
0.8
10^{-3}
10^{-2}
10^{-1}

Figure 8a

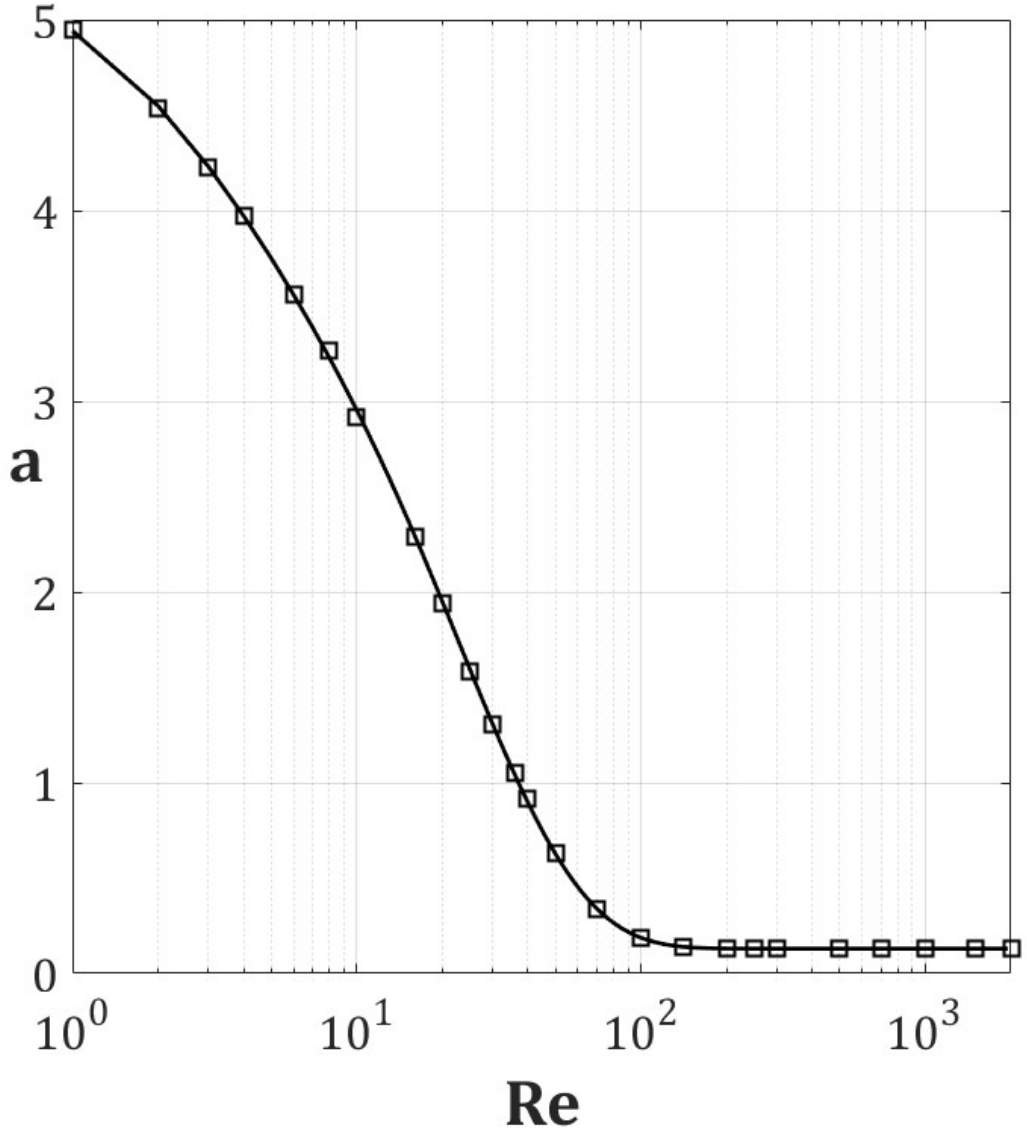

Figure 8b

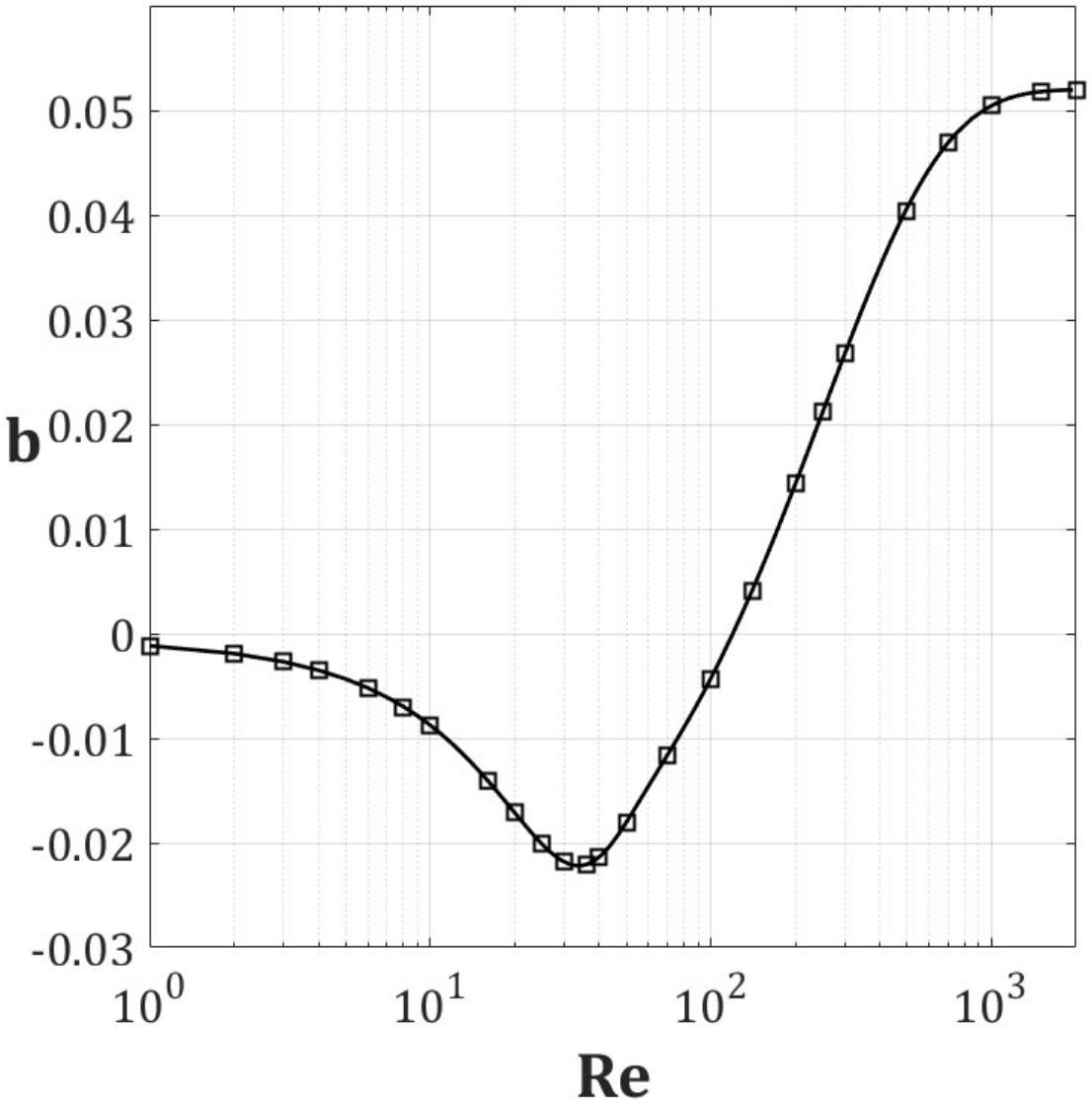

Figure 8c

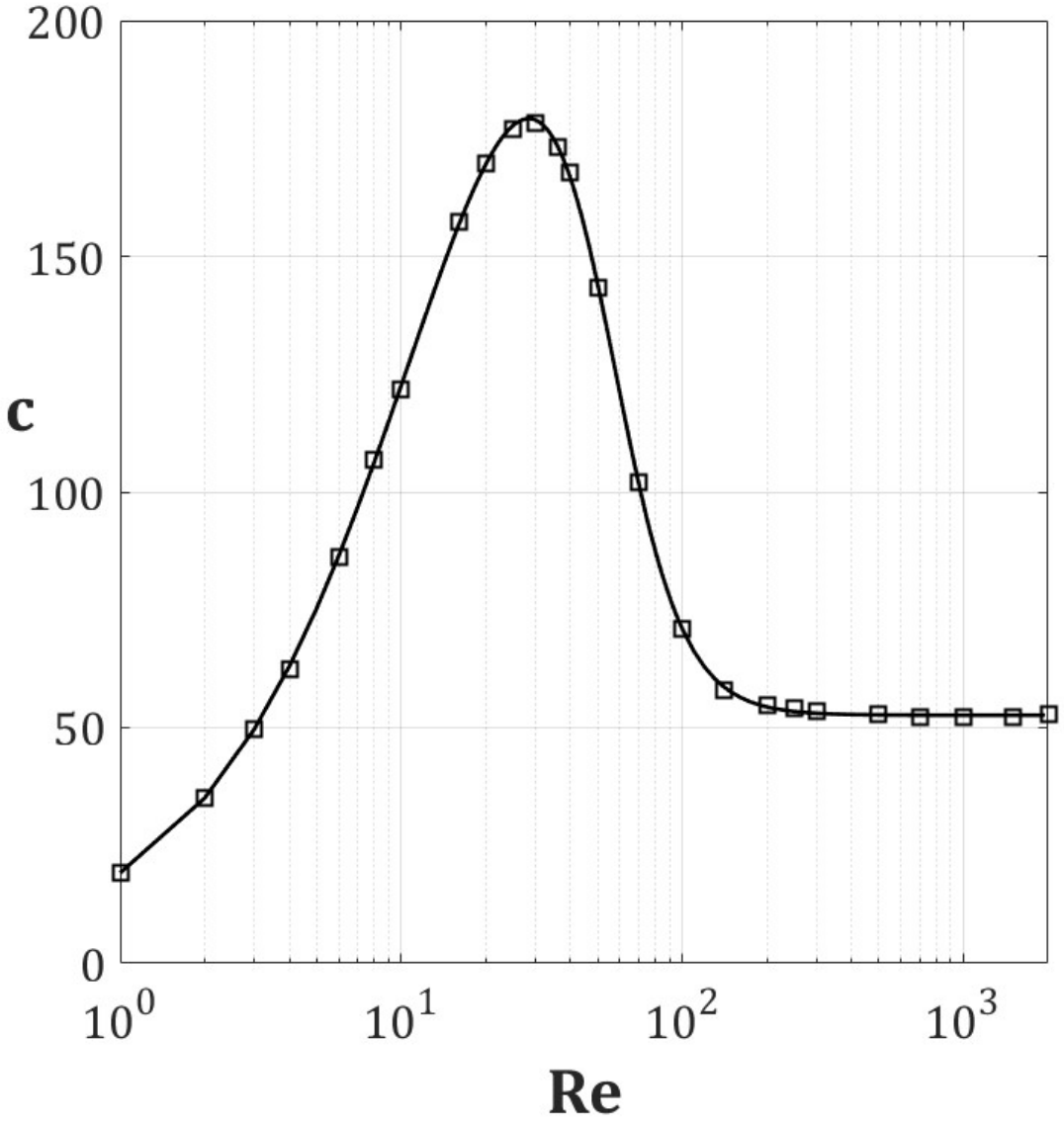

Figure 9

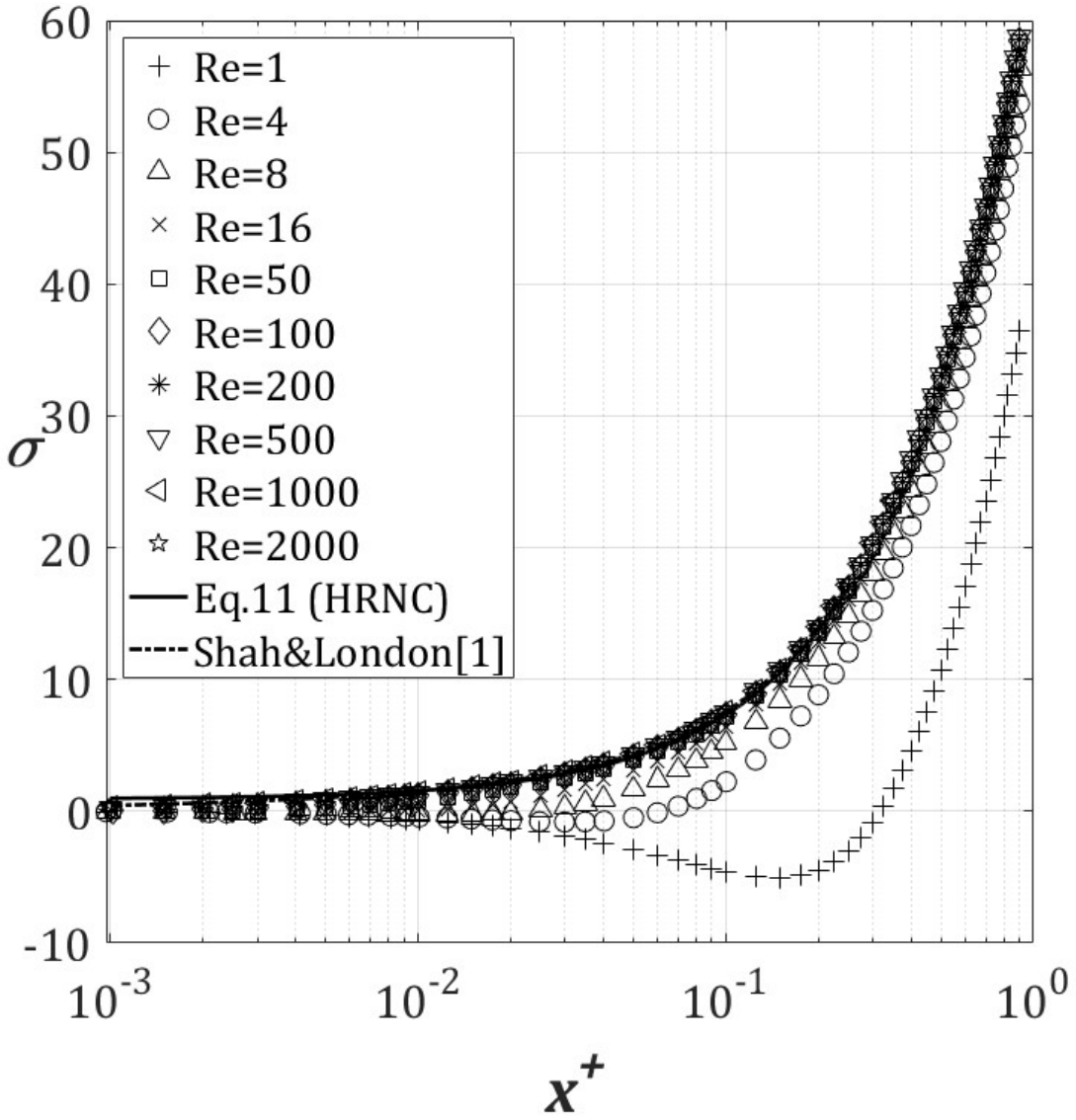
Re=1
Re=4
Re=8
Re=16
Re=50
Re=100
Re=200
Re=500
Re=1000
Re=2000
Eq.11 (HRNC)
Shah&London[1]
60
50
40
30
20
10
0
-10
σ
10^{-3}
10^{-2}
10^{-1}
10^{0}
x^+

Figure 10a

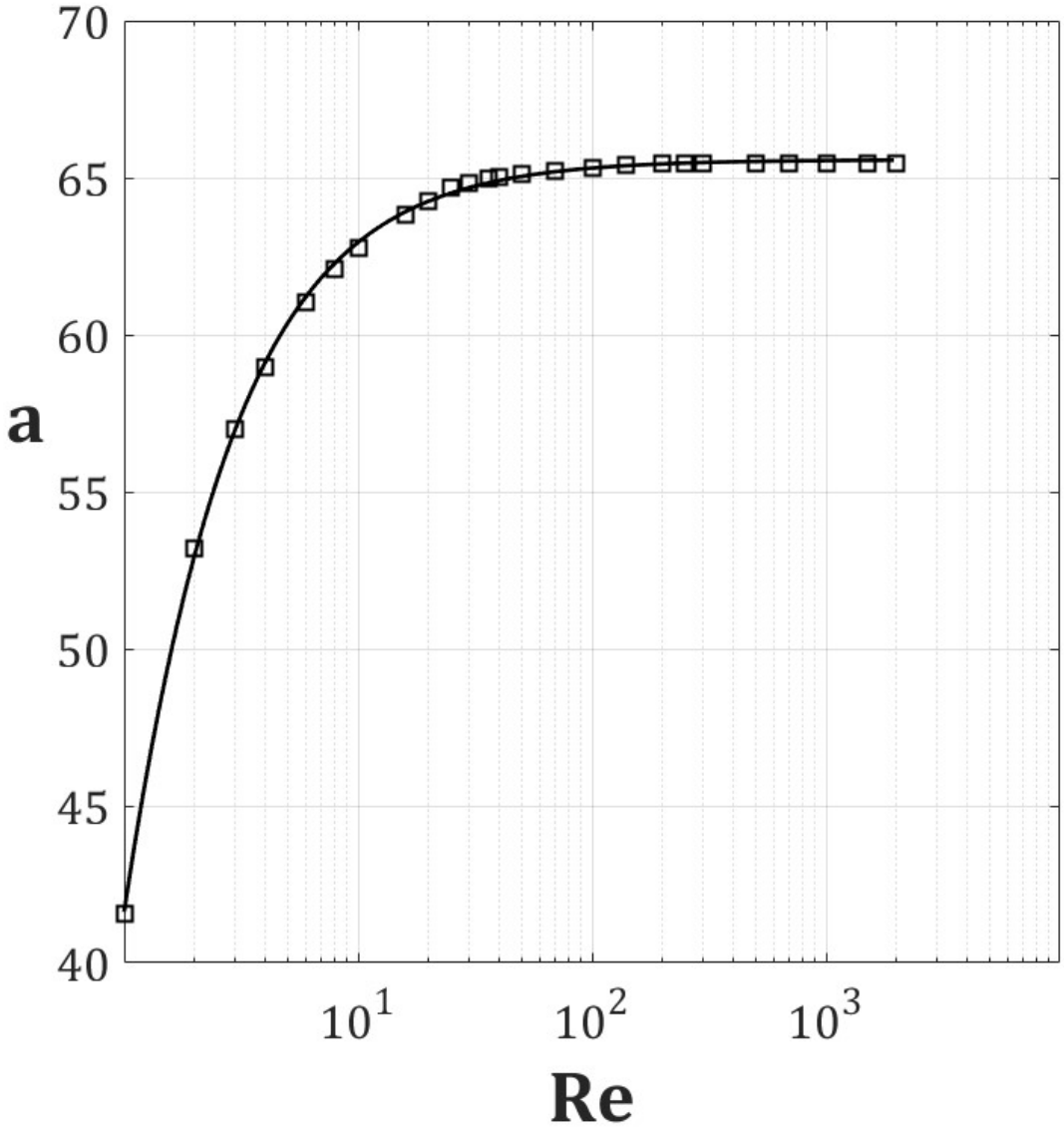

Figure 10b

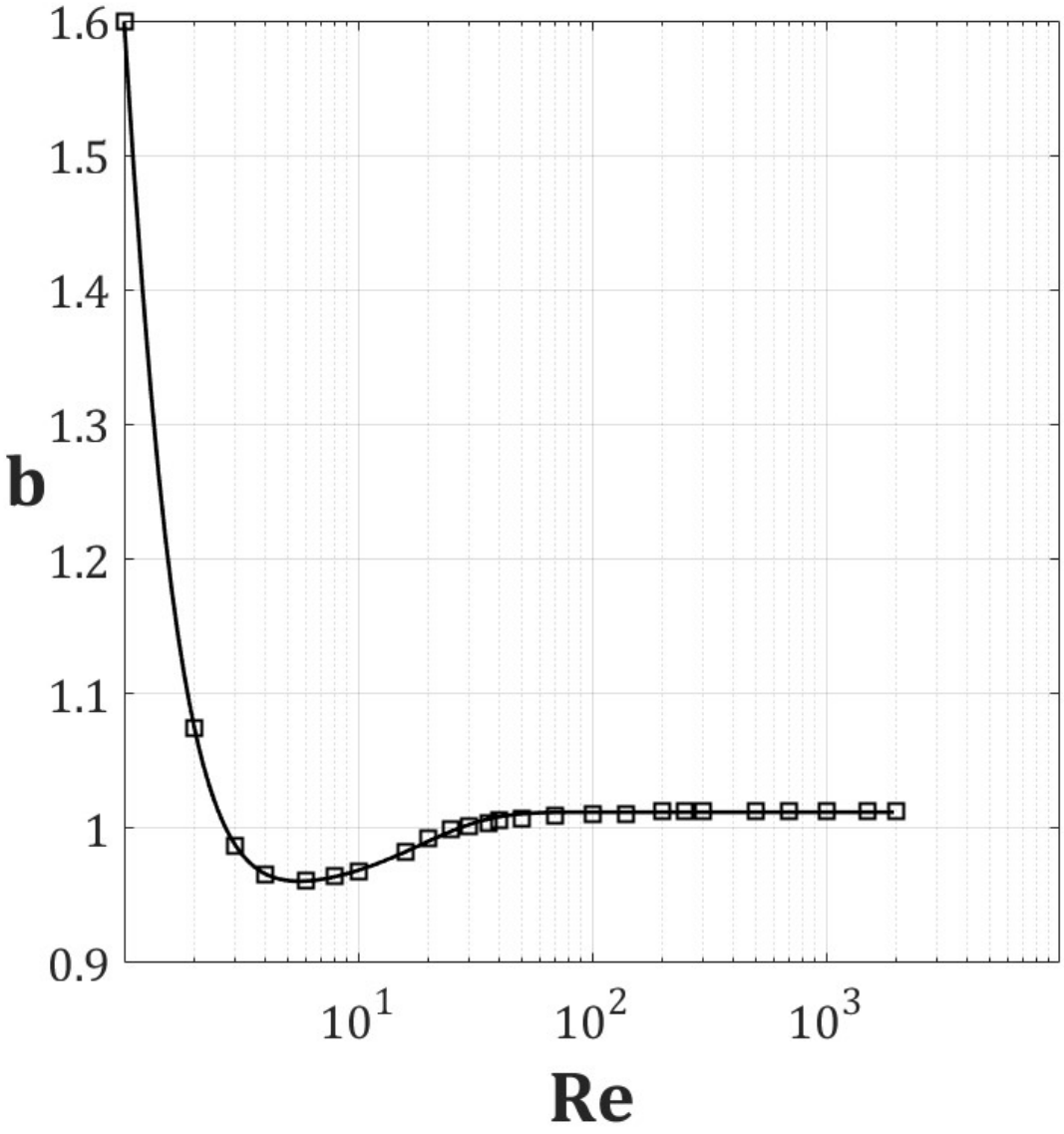

Figure 10c

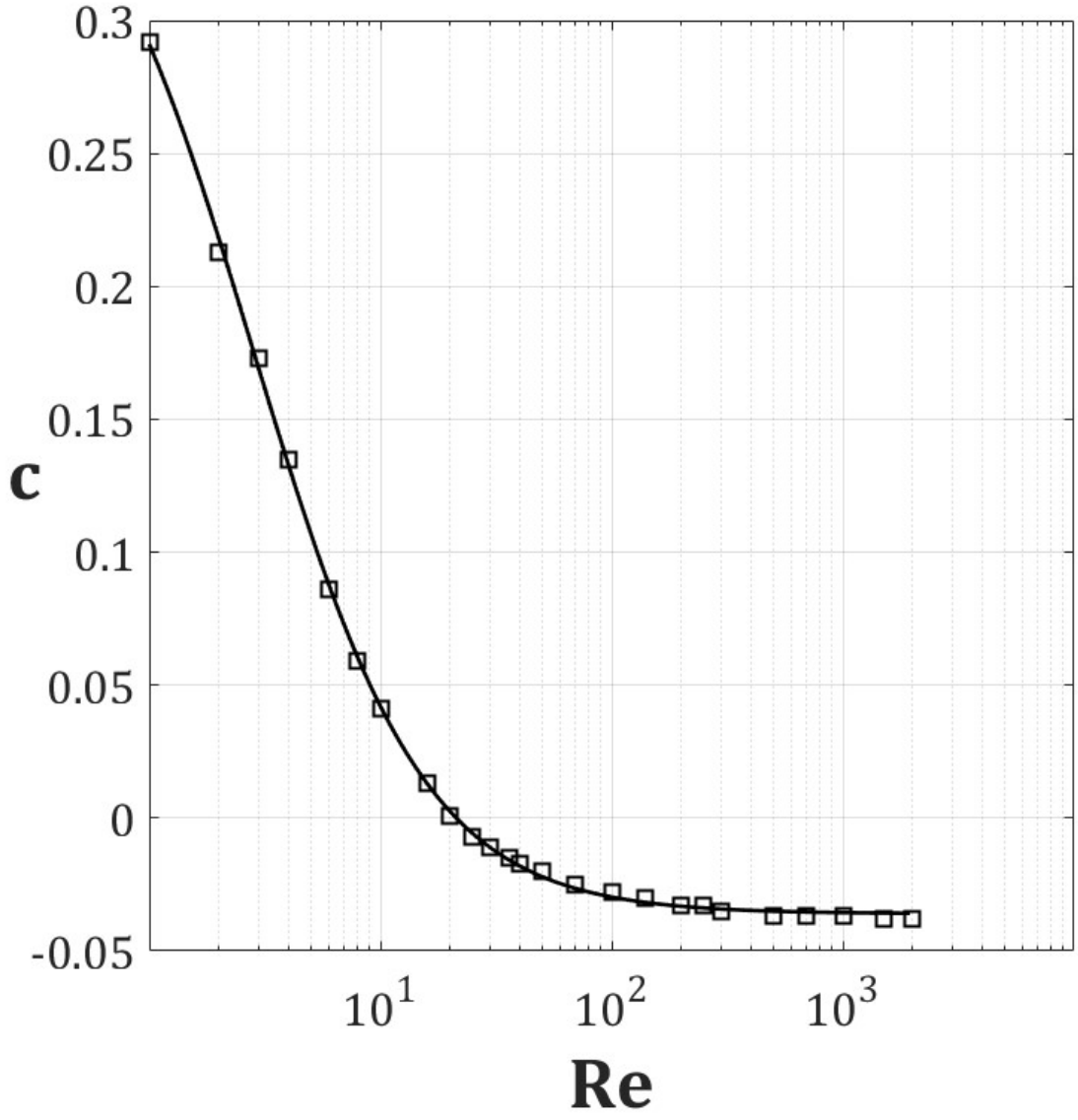

Figure 10d

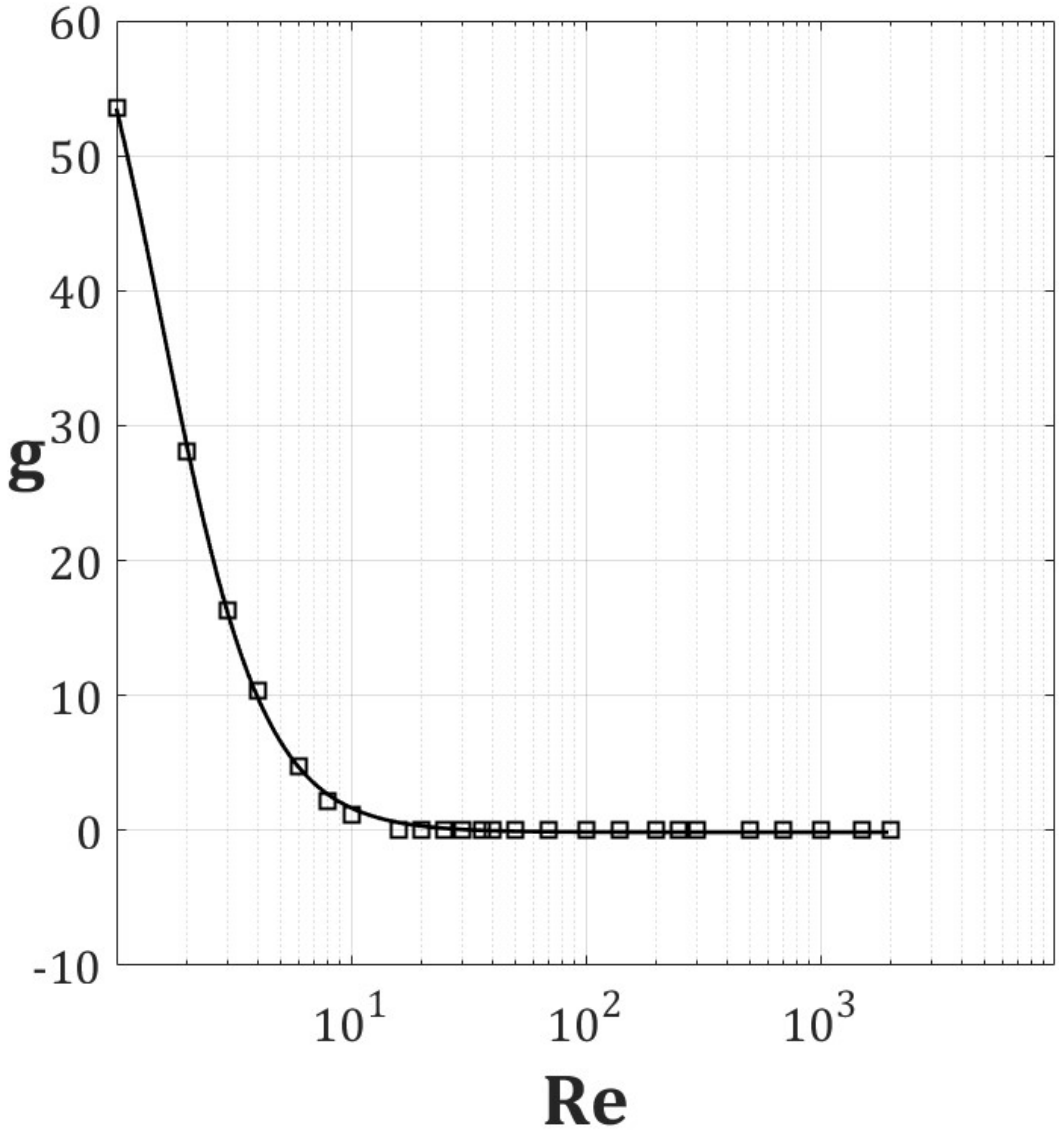

Figure 10e

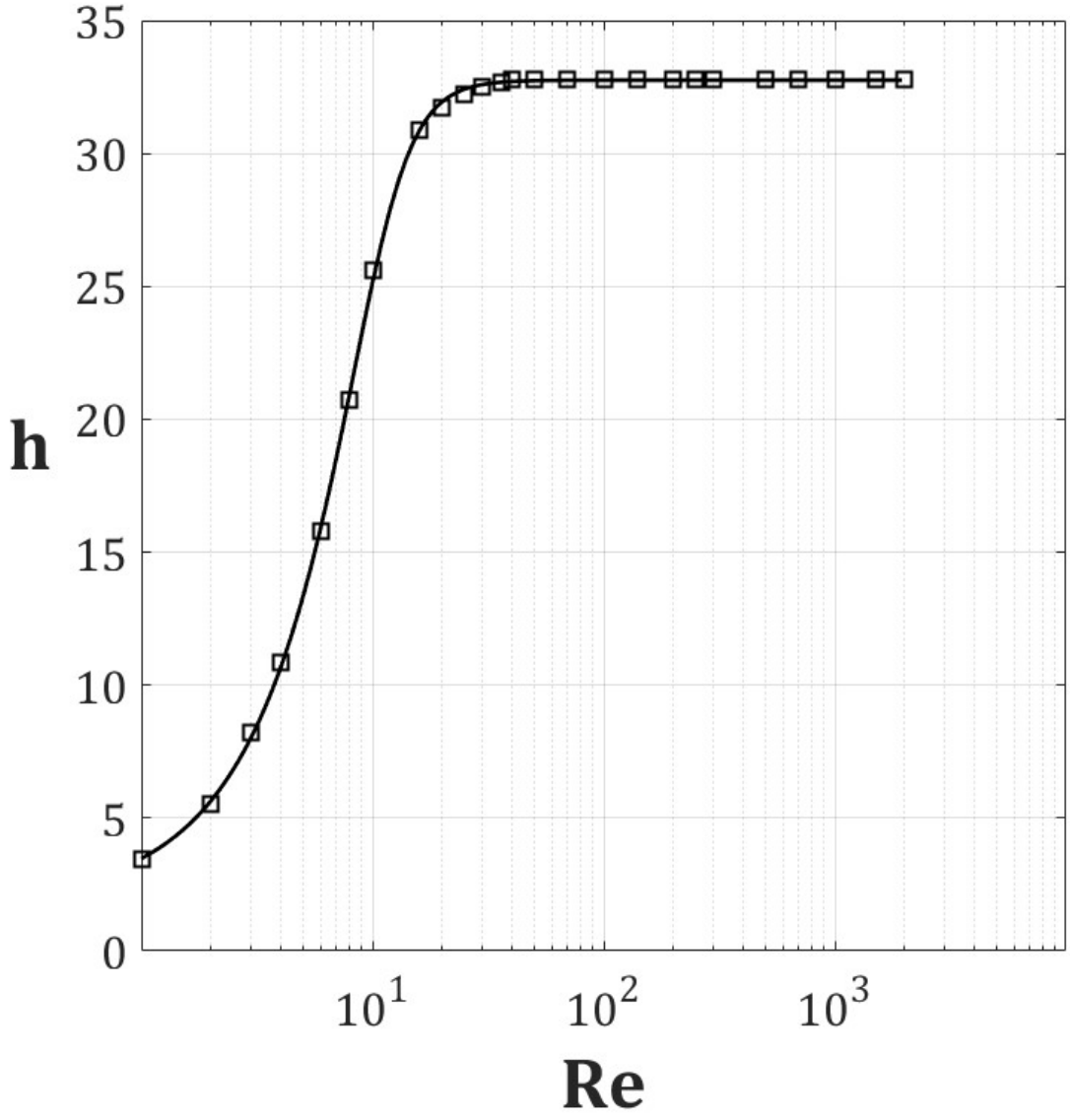

Figure 11

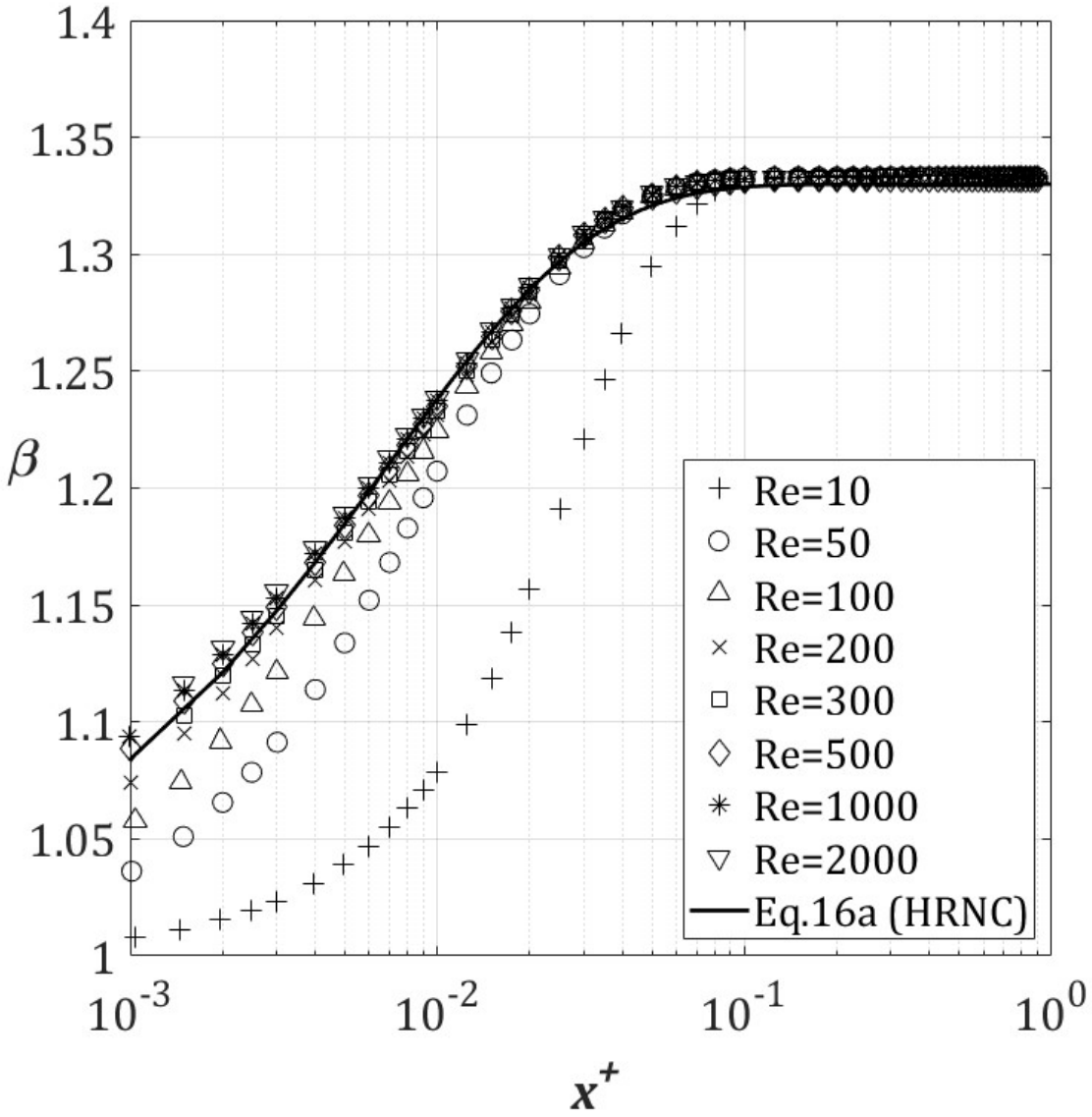
1.4
1.35
1.3
1.25
1.2
1.15
1.1
1.05
1
β
10^-3
10^-2
10^-1
10^0
x+
Re=10
Re=50
Re=100
Re=200
Re=300
Re=500
Re=1000
Re=2000
Eq.16a (HRNC)

Figure 12

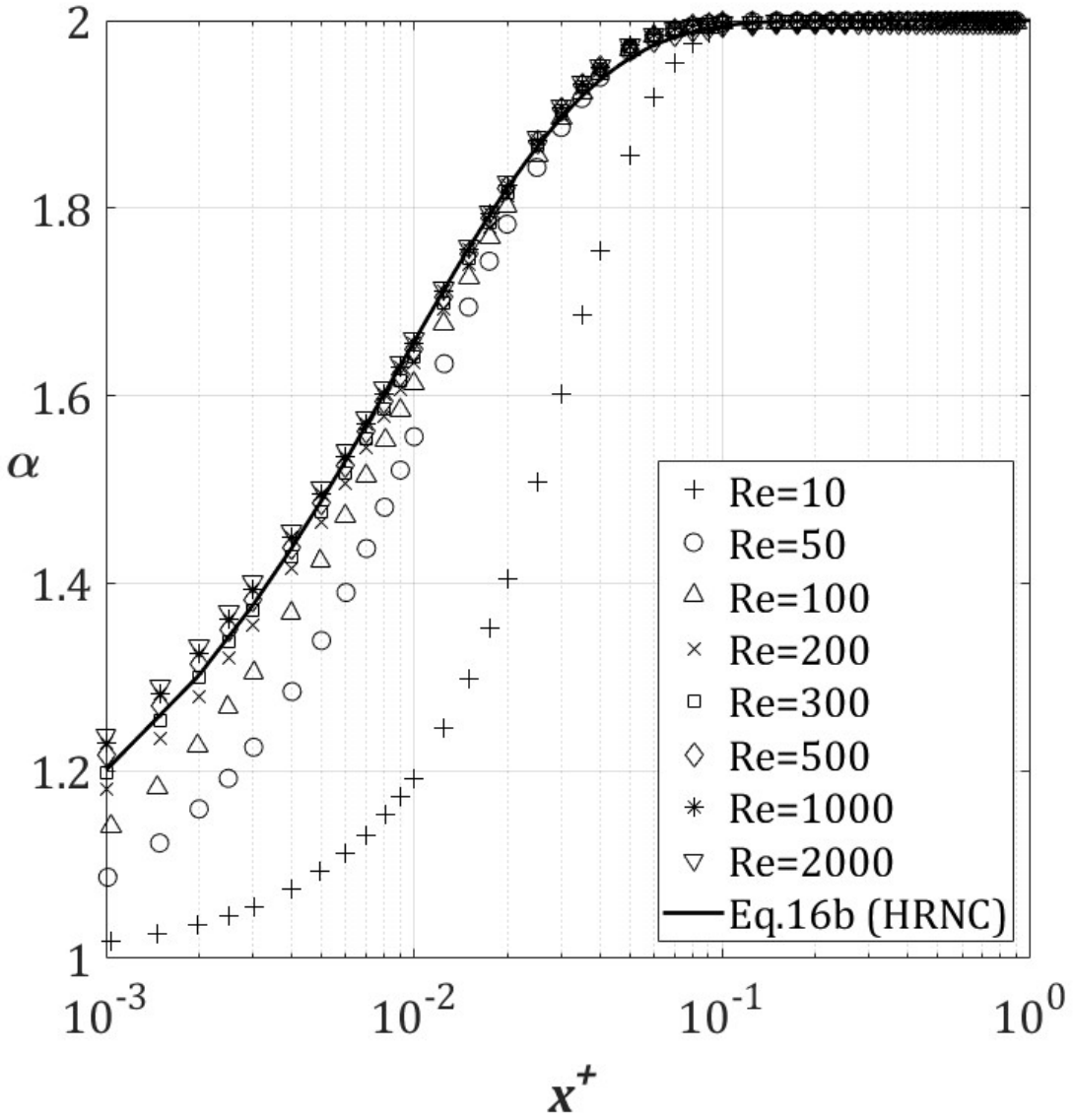
2
1.8
1.6
1.4
1.2
1
α
10^-3
10^-2
10^-1
10^0
x+
Re=10
Re=50
Re=100
Re=200
Re=300
Re=500
Re=1000
Re=2000
Eq.16b (HRNC)

Figure 13a

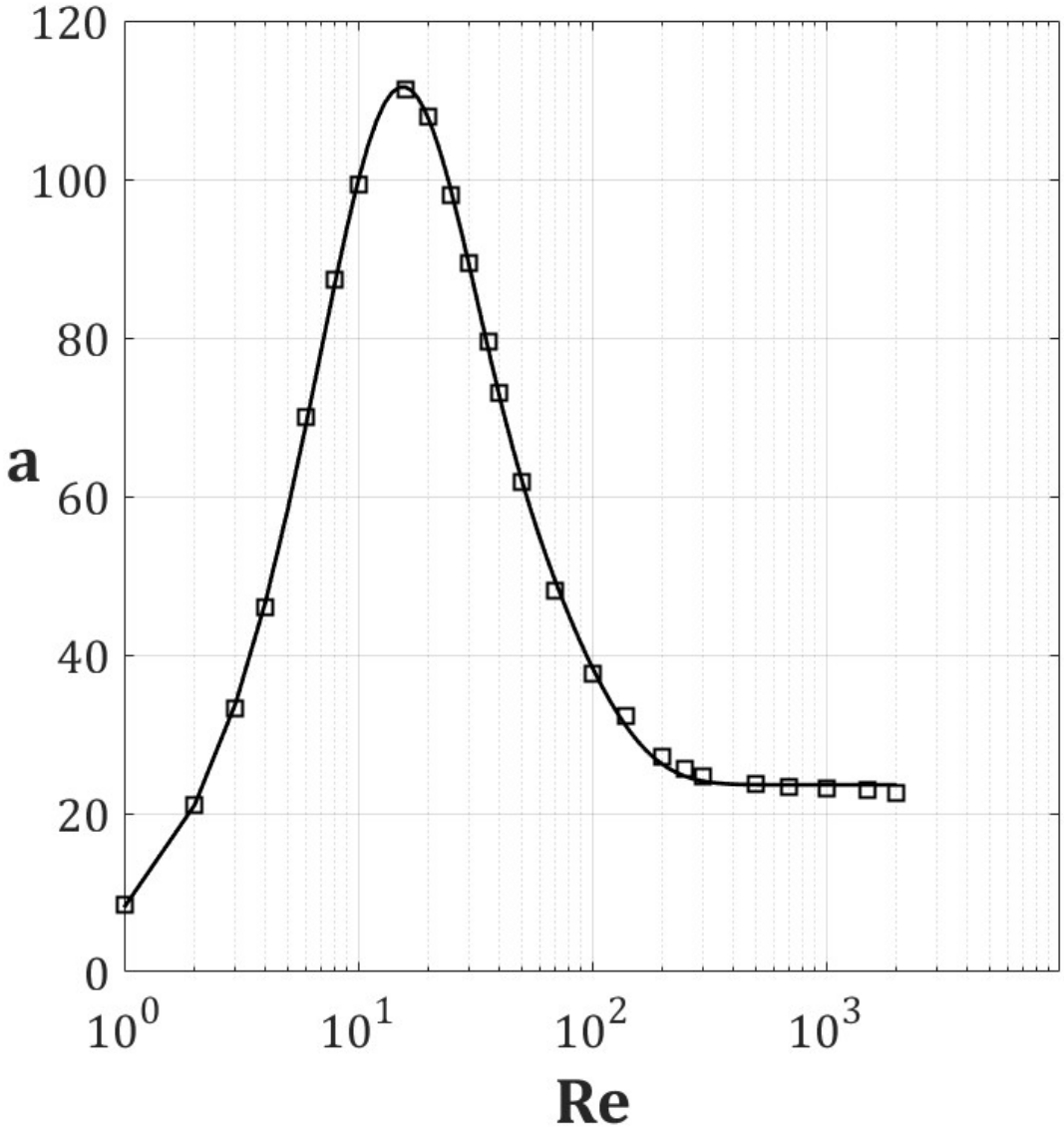

Figure 13b

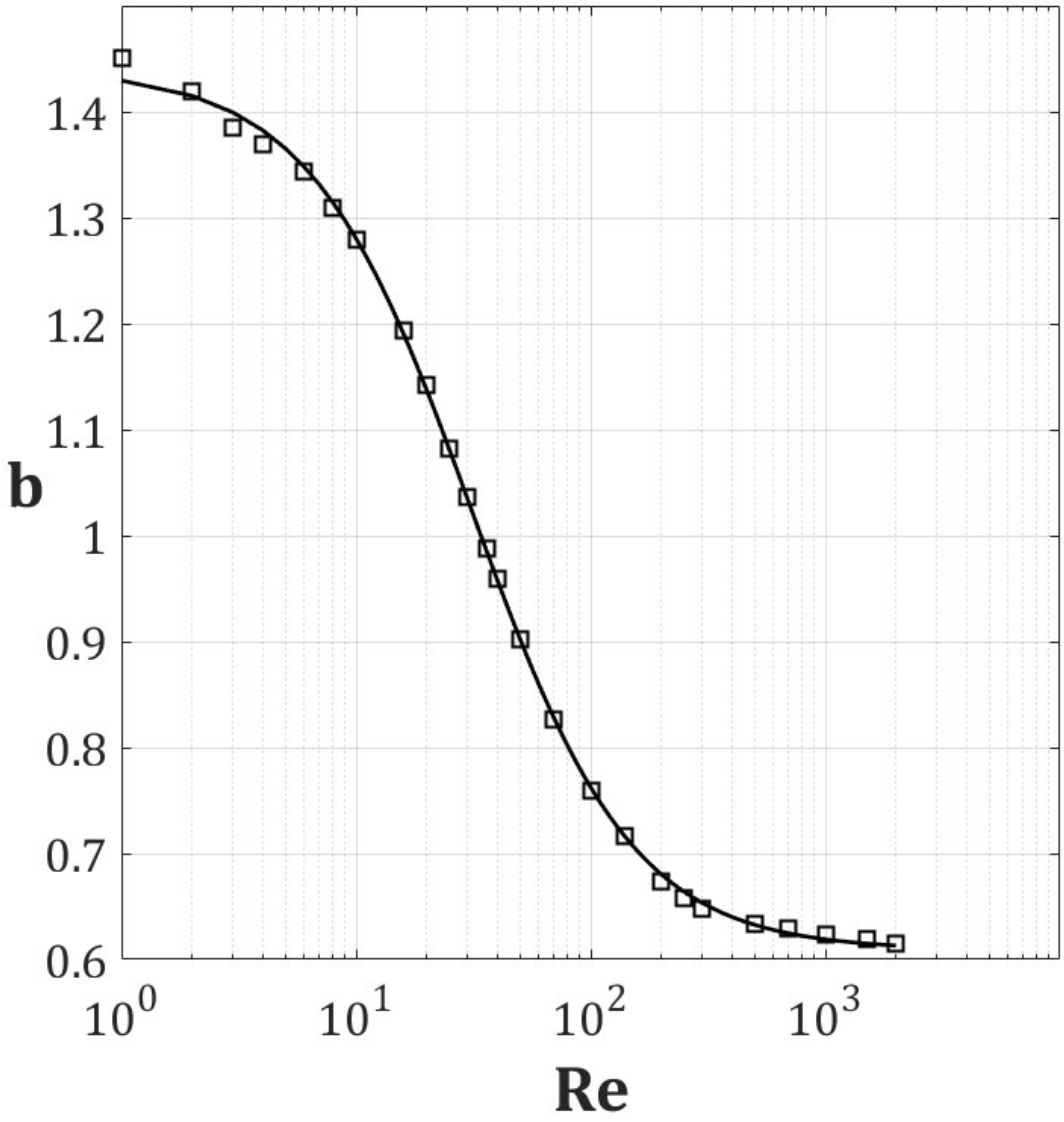

Figure 14a

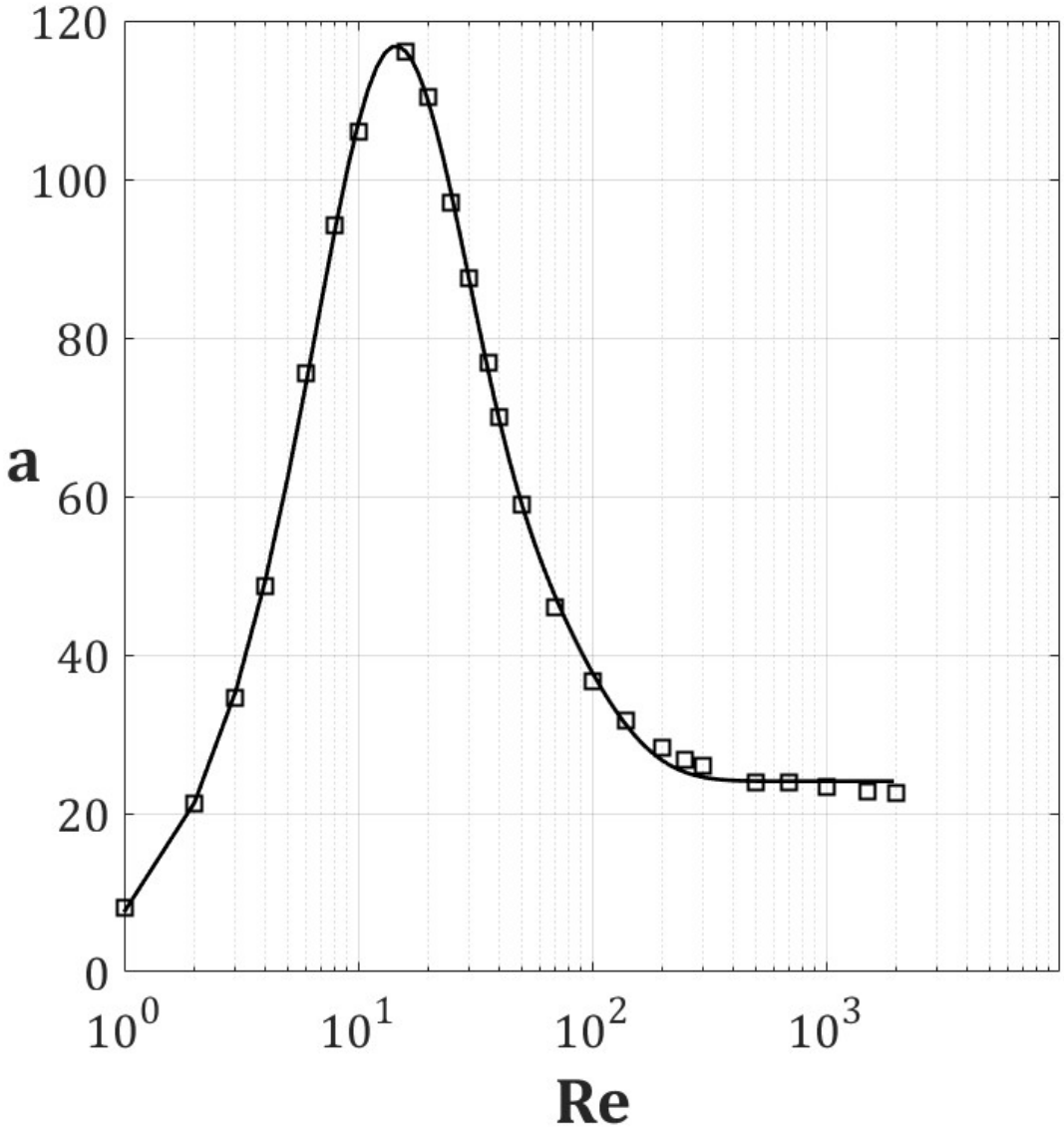

Figure 14b

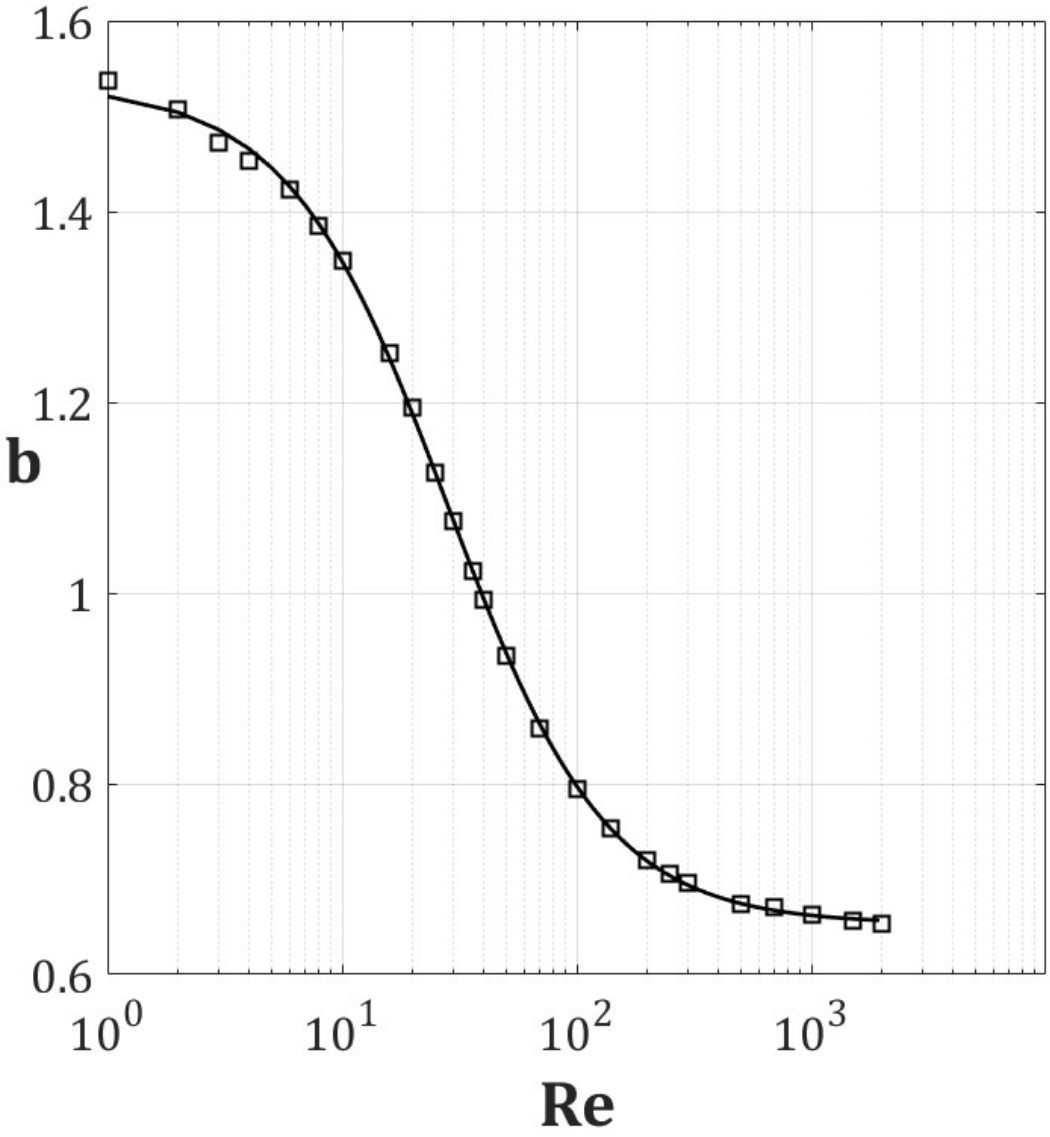

Table 1

Mesh	Number of elements	c_f/c_{f0} ($x^+ = 0.005$)	Grid Convergence Index (GCI)	Lower bound	Upper bound
Coarse	588 552	53.653	-	-	-
Fine	1 150 500	53.567	0.0007	53.566	53.568